Contract No:

This document was prepared in conjunction with work accomplished under Contract No. DE-AC09-08SR22470 with the U.S. Department of Energy.

Disclaimer:

A Thermal Model of the Immobilization of Low-Level Radioactive Waste as Grout in Concrete Vaults

Martin A. Shadday Jr.

Savannah River National Laboratory, Aiken, SC 29808, U. S. A.

Abstract

Salt solution will be mixed with cement and flyash/slag to form a grout which will be immobilized in above ground concrete vaults. The curing process is exothermic, and a transient thermal model of the pouring and curing process is herein described. A peak temperature limit of 85º C for the curing grout restricts the rate at which it can be poured into a vault. The model is used to optimize the pouring.

1. Introduction

The legacy of approximately forty years of producing plutonium and tritium in nuclear reactors at the Savannah River Site is approximately 140,000 m^3 of radioactive waste, which is stored in underground tanks. Most of this waste will be treated by a solvent extraction process which will produce two streams: high-level waste which will be vitrified, and low-level salt solution which will be combined with cement and a flyash/slag mixture to form a leach resistant solid waste form. The grout formed with the low-level salt solution, cement, and flyash/slag is termed saltstone, and it is poured into large concrete vaults for permanent disposal. When a vault is filled, it will be covered with a waterproofed concrete cap and subsequently covered with soil. The combination of the saltstone waste form and the concrete vault will essentially immobilize the low-level waste and thereby protect the groundwater from both chemical and radioactive

contamination. The radioactive liquid waste processing will produce approximately 450,000 m^3 of low-level salt solution, and the volume ratio of saltstone to salt solution is approximately 1.6.

The saltstone curing process involves exothermic reactions, and there is a maximum allowable temperature limit for the saltstone of 85º C. Temperatures above this limit significantly increase the hydraulic conductivity of the saltstone, compromising the integrity of the waste disposal site. The combination of the large volume in a vault and the low thermal conductivity of saltstone promotes high curing temperatures, and the temperature limit therefore restricts the rate at which saltstone can be poured in a single vault. This paper describes a transient thermal model of the saltstone pouring process. The model predicts transient vertical temperature distributions in the saltstone as it is poured into a vault. The objective is to allow optimization of the pour schedule for throughput while maintaining the saltstone peak curing temperature below the temperature limit.

2. Saltstone Pouring Process

The high level waste stored in underground tanks consists of insoluble sludge, less than ten percent of the volume, saltcake, and salt solution. The two salt components are ultimately destined to be immobilized as saltstone. They contain approximately 200 million Curies with ^{137}Cs the major contributor. Most of the radionuclides in the dissolved saltcake and supernate will be removed by a solvent extraction process in the Salt Waste Processing Facility, SWPF. The low-volume high activity waste stream from

the SWPF will be sent to a vitrification facility, and the high-volume low activity salt solution will be sent to the Saltstone Facility. The salt solution is mixed with a dry mixture of flyash, furnace slag, and cement to form grout. This grout is pumped into a concrete vault where it solidifies as a saltstone monolith. The SWPF will have a capacity of 757.1 m^3/wk of salt solution which will result in 1211.4 m^3/wk of grout. The grout pumping capacity is 40.88 m^3/hr; therefore at least thirty hours of pouring per week will be required to meet the SWPF throughput capacity.

The existing vault consists of twelve cells, each 30.48 m square, in which saltstone is poured to a depth of 7.62 m. Fig. 1 is a schematic of the vault in which the roof is partially cut away to show the interior cells. Fig. 2 shows a vertical cross-section of a single cell. The vault roof was originally corrugated metal, and 0.15 m thick layer of concrete was later poured over the metal roof for radiation shielding. The top surface of the roof is coated with a low solar absorptivity coating. The vault bottom is a 0.76 m thick concrete pad that is at ground level, and it rests on a 0.30 m thick layer of gravel and a 0.61 m thick layer of clay. The cells are not forced ventilated. Though this vault has been in existence since the late eighties, it is less than half filled because the SWPF is not operational. An interim solvent extraction facility with a lower capacity than the SWPF has recently become operational, and pouring in earnest should begin in the near future.

There are two sources of internal heat generation within the saltstone: exothermic curing reactions and the decay of radionuclides. Energy from exothermic curing reactions is

dominant during the curing transient. Most of the energy due to curing the saltstone is released within thirty hours of mixing and pouring, but measurable heat generation continues for another six weeks or longer. The temperature limit for curing saltstone is 85º C, and, because of the large volume of saltstone in a single cell and the low saltstone thermal conductivity, the temperature limit restricts the pour rate into a single cell. The Saltstone Facility throughput can be increased by rotating the pouring among several cells.

The allowable Curie content of salt solution going to the Saltstone Facility is 7.57×10^{-4} Curies/m^3 of ^{137}Cs and an overall Curie content of 1.968×10^{-3} Curies/m^3. With saltstone at the allowable Curie limit, the vault roof does not provide sufficient shielding from the radioactivity of multiple cells. Vertical gamma radiation from the top surface of the saltstone in the vault interacts with atoms in the atmosphere, primarily water vapor, and induces secondary radiation. The secondary omnidirectional radiation, "sky shine", poses a hazard on the ground surrounding the vault. The "sky shine" radiation intensity is proportional to the horizontal surface area of the saltstone. To minimize exposure to this radiation, a 0.3048 m thick shield layer of cement will be poured over the saltstone in a vault cell before moving the pouring to an adjacent cell. At any time, only one unshielded cell will be radiating vertically.

The anticipated required vault volume, 720,000 m^3, significantly exceeds the available storage volume in the existing vault; therefore additional vaults will be constructed as the need for additional storage space occurs. The new vaults will consist of pairs of

reinforced concrete tanks placed in an excavated depression in the ground, as shown in Fig. 3. The tank dimensions will be: an inside diameter of 45.72 m and a height of 7.62 m. The thickness of the tank roof will be 0.20 m, and it will be covered with a low solar absorptivity coating. Saltstone will be poured to a depth of 6.07 m.

3. Model Description

The saltstone slab in a cell in the existing vault will be 30.48 m square and, when pouring is finished, 7.62 m thick. The aspect ratio of the slab, thickness to width, is low and saltstone has a low thermal conductivity, so the influence of side wall heat losses will be confined to the vicinity of the walls. The primary heating mechanism is exothermic reactions during the curing process, and the peak temperature will occur in the central region of the saltstone slab where edge losses are negligible. The heat transfer in the central region of the saltstone slab will therefore be essentially one-dimensional in the vertical direction, into the ground below the vault and the air space above the saltstone. The one-dimensional aspect of the heat transfer is used advantageously in thermal modelling of the saltstone pouring process. The model predicts vertical temperature distributions in the saltstone during both the pouring phase and after the cell is filled.

This is a one-dimensional transient finite-difference heat conduction model with a variable mesh and a moving boundary at the top. The computational domain extends twenty-five meters into the ground below the vault, where the bottom boundary is assumed to be adiabatic. The air space in a vault cell is treated as a well-mixed control volume, and thermal conduction through the vault roof is treated in the same manner as in

the saltstone. The top surface of the vault roof is subjected to both convection and radiation heat transfer with the environment. Ventilation of the air space by outside air is allowed for in the model, but it is generally assumed to be zero. Fig. 4 is a schematic of a vault cell showing the heat transfer phenomena to which the saltstone is subjected. Both the diurnal and annual variations in the ambient air temperature are included in the model. During the day, the roof is assumed to be exposed to solar radiation with insolation typical of a sunny spring or autumn day.

The finite-difference equations are formulated with either the Crank-Nicolson semi-implicit or a fully-implicit numerical scheme. The Thomas algorithm (Anderson et al. 1984) is used to solve the resultant tri-diagonal system of equations. The mesh-width for the saltstone is the thickness of a layer of saltstone in a cell poured in one hour, and one hour is the fixed time-step size. The saltstone mesh-width determines whether the semi-implicit or fully-implicit formulation is utilized. Because of the low thermal conductivity of saltstone, the semi-implicit formulation is generally stable with a one hour time-step, but if the pour rate is sufficiently slow such that the small mesh-width reduces the maximum stable time-step size below one hour, the fully implicit formulation is used. A variable mesh-width is used in the foundation and ground below the vault

Eq. (1) is the governing equation for one-dimensional transient heat conduction with internal heat generation. The finite-difference equations are derived with the control volume approach. Fig. 5 shows three adjacent interior nodes in a one-dimensional variable-width mesh, and Eq. (2) is the semi-implicit form of the finite difference

equation for the i^{th} node. The thermal conductivities are equivalent thermal conductivities for the cases where adjacent control volumes contain different materials. This occurs in the ground below the vault at the interfaces between the soil, the vault foundation materials and the saltstone. Eq. (3) is the expression for the equivalent thermal conductivity between the *i-1* and i^{th} nodes.

$$\frac{\partial}{\partial z}\left(k\frac{\partial T}{\partial z}\right)+q^{*}=\rho C_{p}\frac{\partial T(z,t)}{\partial t} \tag{1}$$

$$\begin{aligned}\left(\rho C_{p}\Delta z\right)_{i}A\frac{T_{i}^{n+1}-T_{i}^{n}}{\Delta t}=-k_{i-1,i}A\frac{\frac{1}{2}\left(T_{i}^{n+1}+T_{i}^{n}\right)-\frac{1}{2}\left(T_{i-1}^{n+1}+T_{i-1}^{n}\right)}{\frac{1}{2}\left(\Delta z_{i-1}+\Delta z_{i}\right)}+\\ k_{i+1,i}A\frac{\frac{1}{2}\left(T_{i+1}^{n+1}+T_{i+1}^{n}\right)-\frac{1}{2}\left(T_{i}^{n+1}+T_{i}^{n}\right)}{\frac{1}{2}\left(\Delta z_{i+1}+\Delta z_{i}\right)}+\left(\rho\Delta zAq^{*}\right)_{i}\end{aligned} \tag{2}$$

$$k_{eq}=\frac{k_{i}k_{i-1}\left(\Delta z_{i}+\Delta z_{i-1}\right)}{\Delta z_{i}k_{i-1}+\Delta z_{i-1}k_{i}} \tag{3}$$

Eq. (4) is a general semi-implicit finite-difference equation. This equation is stable as long as the coefficients of the previous time level variables on the right-hand side of the equation are positive (Lax and Richtmyer 1956). The coefficient of T_i^n, when Eq. (2) is put in the same format as Eq. (4), can be negative for large values of the time-step. Eq. (5) is the expression for the maximum stable time-step for Eq. (2). If Δt_{max} is less than one hour, the fully-implicit form of Eq. (2), in which the conduction terms on the right side of the equation are expressed in terms of the *n+1* time level only, must be used. This form of the finite-difference equations is unconditionally stable.

$$a_{i-1}\phi_{i-1}^{n+1}+a_{i}\phi_{i}^{n+1}+a_{i+1}\phi_{i+1}^{n+1}=b_{i-1}\phi_{i-1}^{n}+b_{i}\phi_{i}^{n}+b_{i+1}\phi_{i+1}^{n} \tag{4}$$

$$\Delta t_{\max}=\frac{\left(\rho C_{p}\Delta z\right)_{i}\left(\Delta z_{i+1}+\Delta z_{i}\right)\left(\Delta z_{i-1}+\Delta z_{i}\right)}{k_{i-1,i}\left(\Delta z_{i+1}+\Delta z_{i}\right)+k_{i+1,i}\left(\Delta z_{i-1}+\Delta z_{i}\right)} \tag{5}$$

The finite-difference equations for the top saltstone node and the bottom soil node differ from Eq. (2) because of the applied boundary conditions. The bottom boundary is adiabatic and the top node is subjected to heat transfer. Eqs. (6) and (7) are the semi-implicit forms of the bottom and top nodal equations respectively. The top loss heat transfer rate term is evaluated separately and specified in the calculation of the temperature distribution in the saltstone and the ground below the vault. If pouring is taking place, $\dot{q}_{top}$ is the thermal conduction heat transfer rate to the pour layer, otherwise it is the sum of the heat transfer loss rates by thermal convection and radiation from the surface of the saltstone. The temperature of the pour layer is calculated separately from the previously poured saltstone temperature distribution.

$$\left(\rho C_p \Delta z\right)_1 \frac{T_1^{n+1} - T_1^n}{\Delta t} = k_{1,2} A \frac{\frac{1}{2}\left(T_2^{n+1} + T_2^n\right) - \frac{1}{2}\left(T_1^{n+1} + T_1^n\right)}{\frac{1}{2}\left(\Delta z_1 + \Delta z_2\right)} + \left(\rho \Delta z\right)_1 A q_1^* \qquad (6)$$

$$\left(\rho C_p \Delta z\right)_{i\max} A \frac{T_{i\max}^{n+1} - T_{i\max}^n}{\Delta t} = k_{im,i\max} A \frac{\frac{1}{2}\left(T_{im}^{n+1} + T_{im}^n\right) - \frac{1}{2}\left(T_{i\max}^{n+1} + T_{i\max}^n\right)}{\frac{1}{2}\left(\Delta z_{im} + \Delta z_{i\max}\right)} + \left(\rho \Delta z A q^*\right)_{i\max} - A\dot{q}_{top} \qquad (7)$$

The set of Eqs. (2) (6) and (7) are "imax" simultaneous linear equations for the updated temperature distribution in the saltstone and the ground below the vault. The set of equations has a tridiagonal coefficient matrix, as shown in Eq. (8), and it is solved directly with the Thomas algorithm (Anderson et al. 1984).

$$\begin{bmatrix} d_1 & c_1 & 0 & 0 & 0 \\ a_1 & d_2 & c_2 & 0 & 0 \\ 0 & \ddots & \ddots & \ddots & 0 \\ 0 & 0 & a_{im-1} & d_{im} & c_{im} \\ 0 & 0 & 0 & a_{im} & d_{i\max} \end{bmatrix} \begin{Bmatrix} T_1^{n+1} \\ T_2^{n+1} \\ \vdots \\ T_{im}^{n+1} \\ T_{i\max}^{n+1} \end{Bmatrix} = \begin{Bmatrix} b_1 \\ b_2 \\ \vdots \\ b_{im} \\ b_{i\max} \end{Bmatrix} \qquad (8)$$

The saltstone curing process is exothermic. Fig. 6 shows the empirically determined internal heat generation rate, due to the saltstone heat of hydration, as a function of elapsed time after mixing. The large spike in internal heat generation power is termed the second heat of hydration and the saltstone setting occurs simultaneous with this spike. Each saltstone node represents a layer of saltstone poured in one hour, and the source term is the integrated average value the heat of hydration for the hour bracketing the elapsed time since pouring of the layer. The heat of hydration is the dominate contributor to the internal heat generation source term. An adiabatic calorimeter was used determine the heat of hydration, and the temperature exceeded 100º C. Also the salt solution was a non-radioactive stimulant of actual waste. The heat of hydration is a function of temperature and the composition of the salt solution. An earlier test, in which real saltstone was poured into a hole with both a depth and diameter of 1.83 m and a thermocouple tree, produced a heat of hydration with a total energy release of approximately 85% of the energy released by the calorimeter test described above. The peak temperature of the saltstone was less than 70º C.

In addition to the heat of hydration, there is internal heat generation due to decay of the radionuclides in the salt solution. The allowable radionuclide deposited power in the saltstone is 1.9653×10^{-4} W/kg. This is the total decay power of a mixture of thirty-seven isotopes. Most of this power (71%) comes from the decay of ^{137}Cs which has a half-life of 30.17 years. Decay of the radiolytic deposited power is not important for the pour transient, the duration of which is generally less than two years, but it can be important for long multi-year transient calculations. A simplified scheme is used to

account for decay. Radionuclides with half-lives less than 15 years (20.9 %) are lumped together and assumed to have a 7.5 year half-life, radionuclides with half-lives between 15 and 100 years (75.0 %) are assumed to have a 30 year half-life, and radionuclides with half-lives greater than 100 years (4.1 %) are assumed to have a very long half-life.

Fig. 7 is a schematic of the pour layer, showing the heat transfer mechanisms considered in the model. Heat is conducted into the pour layer from the saltstone below, and heat is lost from the surface by natural convection with the vault air space and thermal radiation to the vault ceiling. The surface of the saltstone is assumed to be at the pour temperature, and this temperature is used to calculate the convection and radiation heat loss rates. Thermal conduction from the saltstone is defined in terms of the pour layer temperature. Eq. (9) is an energy balance for the pour layer. The saltstone surface temperature used to determine the convection and radiation heat transfer rates is the pour temperature. The convection heat transfer is with the vault airspace and radiation heat transfer is with the underside of the vault ceiling.

$$\rho C_p \Delta z \frac{T_{pl} - T_{pour}}{\Delta t} = \frac{k_{ss}\left(T_{i\max} - T_{pl}\right)}{\Delta z} - \dot{q}_{conv} - \dot{q}_{rad} \qquad (9)$$

When a new layer of saltstone is poured onto cured saltstone, there is potentially a thermal contact resistance due to poor bonding between the cured and freshly poured saltstone. These contact resistances occur between layers of saltstone poured on different days, and they effectively lower the thermal conductivity of the saltstone. The impact of a 0.1 mm contact resistance air gap between layers of saltstone 0.3048 m thick is to lower the thermal conductivity by 1.2%. This is assuredly well within the uncertainty in the

value of the saltstone thermal conductivity, and therefore contact resistances are ignored in the model.

The air space is treated as a single control volume. Eq. (10) is the finite-difference form of the thermal energy equation for the air space. The fully-implicit form of this equation is used. The last two terms in Eq. (10) are the convection heat transfer rates with the saltstone surface and the underside of the roof respectively, and they are used as boundary conditions for the saltstone and roof thermal conduction calculations.

$$\rho A Z_{airsp} C_p \left(\frac{T_{airsp}^{n+1} - T_{airsp}^{n}}{\Delta t} \right) = \dot{m}_{air} C_p \left(T_{air} - T_{airsp}^{n+1} \right) + h_{ss} A \left(T_{ss} - T_{airsp}^{n+1} \right) + h_{rf} A \left(T_{rf} - T_{airsp}^{n+1} \right) \quad (10)$$

Thermal conduction through the concrete roof is calculated numerically, using fully-implicit finite-difference equations and constant mesh-width and physical properties. The top and bottom boundary nodes have thicknesses of one-half mesh-width and the nodal temperatures are at the respective surfaces, see Fig. 8. The finite-difference equations form a tridiagonal set of simultaneous equations which are solved with the Thomas algorithm (Anderson et al. 1984). The radiation heat transfer boundary conditions for both the bottom and top surfaces are linearized by expressing the heat transfer rates in the form of Newton's law of cooling. The radiation heat transfer between the saltstone and the vault roof is treated as heat transfer between two infinite parallel flat surfaces, Eq. (11). The radiation heat transfer coefficient is calculated with the old value of the roof surface temperature.

$$\dot{q}_{rad} = \frac{\dot{Q}_{rad}}{A} = \frac{\sigma \varepsilon_{ss} \varepsilon_{rf} \left(T_{ss}^2 + T_{rf}^2 \right) \left(T_{ss} + T_{rf} \right) \left(T_{ss} - T_{rf} \right)}{\varepsilon_{ss} + \varepsilon_{rf} - \varepsilon_{ss} \varepsilon_{rf}} = h_{rad} \left(T_{ss} - T_{rf} \right) \quad (11)$$

The upper surface of the vault roof is cooled by the ambient air and thermal radiation with the sky. The daily mean ambient air temperature is assumed to vary sinusoidally ±11.1 ºC about the annual average temperature of 18.3 ºC with the peak temperature on July 16th and the minimum temperature on January 15th. The diurnal temperature variation is assumed to be ±6.7 ºC about the daily mean temperature. The upper surface of the vault roof radiates to a black body at the sky temperature, Eq. (12), both day and night (Duffie and Beckman 1974). During the day, it is exposed to solar radiation with insolation typical for a sunny spring or autumn day. The time dependent solar insolation is shown in Fig. 9. The vault roof has a low solar absorptivity coating.

$$T_{sky} = 0.0552 T_{air}^{3/2} \tag{12}$$

In addition to the air surrounding the vault, the ground below the vault serves as a heat sink for the saltstone. The ground is modelled to a depth of 25.0 meters, and the lower boundary is assumed to be adiabatic. The initial temperature distribution in the ground varies with the time of year that pouring commences. Fig. 10 shows temperature profiles in the ground below an empty cell in the existing vault at four different times of the year. These temperature distributions were determined by running the model, with no saltstone pouring, for 1000 years. This period is long enough such that the vertical temperature profile is independent of the initial assumed temperature profile. The temperature of the top six meters varies on an annual basis, and the temperature of the earth below six meters is constant at approximately 16.5 º C.

The model marches through a transient of specified duration with timesteps of one hour. The pour days and the number of hours of pouring each day are specified in input. The saltstone pour temperature is assumed to be the daily average ambient temperature. Fig. 11 is a flowchart of the model. The computational sequence within a timestep is to first calculate the airspace temperature with Eq. (10). With this updated temperature, the convection heat transfer rates with the saltstone surface and the underside of the vault roof are evaluated. These are boundary conditions for the evaluation of temperature distributions in the saltstone and the roof. Second the roof temperature distribution is evaluated. The radiation heat transfer rate between the saltstone and the underside of the roof is then evaluated. This is a boundary condition for evaluating the pour layer temperature or the saltstone temperature distribution when no pouring is occurring. If pouring is taking place, the pour layer temperature is then evaluated, with Eq. (9), followed by evaluation of the conduction heat transfer rate between the previously poured saltstone and the pour layer. The last step in the computational sequence is to update the vertical temperature distribution in the saltstone and ground below the vault. Before the saltstone temperature distribution is updated, the spatial distribution of the internal heat generation source term is updated. The boundary condition at the top surface is a specified heat transfer rate, either conduction to the pour layer or convection with the airspace and radiation to the roof.

4. Model Verification and Validation

Conservation of energy is necessary though not sufficient to validate a thermal model. The entire vault cell, its contents, and the ground under the vault are considered a control

volume. The change in internal energy is equal to the internal heat generation minus heat losses to the surrounding environment plus the net energy convected into the control volume, Eq. (13).

$$\int \left(\rho C_p T\right)_{final} d\forall - \int \left(\rho C_p T\right)_{initial} d\forall = \iint \rho q^* d\forall dt - \int \dot{Q} dt + \int \sum \left(\dot{m} C_p T\right) dt \qquad (13)$$

The bottom boundary 25.0 m below the vault is assumed to be adiabatic, so the heat transfer with the environment occurs at the top surface of the roof. Energy is convected into the control volume with the poured saltstone, and it is convected out with the air displaced by the pouring saltstone. Results of an energy balance for a case in which saltstone is poured eight hours per day two days a week for eleven weeks, are shown below:

Initial energy	2.0886568×10^{10} J/m^2
Final energy	2.6820628×10^{10} J/m^2
Internal heat generation	1.9096952×10^{9} J/m^2
Roof losses	1.3155690×10^{9} J/m^2
Saltstone pour energy	5.3427039×10^{9} J/m^2
Air space losses	2.7705679×10^{6} J/m^2
Energy balance error	9.4230175×10^{-3} J/m^2

The "energy balance error" is the residual when the terms on the right-hand side of Eq. (13) are brought over to the left side. The ratio of the "energy balance error" to the "final energy" is 3.5×10^{-13}. This is very small, as is the residual, and it is therefore reasonable to conclude that the model conserves energy.

There is a vertical thermocouple array in each cell with thermocouples spaced 0.914 m apart. Between February 10th and March 20th of 2008, saltstone was poured to a depth of 3.048 m in a vault cell. The saltstone pour rate was 35.40 m^3/hr. Pouring occurred on

fourteen days with four hour pours on eight of those days. Fig. 12 shows the transient height of the saltstone surface above the cell bottom. Also shown are the elevations of the three thermocouples that were submerged by the saltstone. Figs. 13 through 15 show the predicted and measured temperatures by the three thermocouples that were covered by saltstone. Prior to being covered by saltstone, the thermocouples indicate the cell airspace temperature. The initial two day pour results in a 0.61 m thick saltstone layer, which does not reach the lowest thermocouple. This thermocouple clearly shows the heating of the airspace by the curing saltstone layer. The approximately 5º C daily oscillation of the airspace temperature is due to the diurnal variation in ambient temperature. The three thermocouples clearly show the dramatic temperature rise of the curing saltstone.

The ambient conditions in the simulation were the standard model conditions, described in the previous section, rather than actual weather data. The actual grout pour temperatures are unknown, and therefore the model daily average ambient temperatures were used. The heat of hydration internal heat generation term in the model was assumed to be 85% of the value from the functional relation shown in Fig. 6. This is reasonable in view of the low curing temperatures in this limited test.

6. Results and Discussion

The saltstone thermal responses to several pour scenarios in the existing vault are presented. In all cases the saltstone pour rate is assumed to be the maximum 0.68137 m^3/min, and at this pour rate the saltstone surface rises at the rate 0.04401 m/hr. A pour

day consists of eight hours of pouring unless fewer hours are required on the last pour day to fill a cell. Before pouring is switched from one cell in the vault to another, a 0.3048 m thick layer of cement, for radiation shielding, is poured over the previously poured saltstone. This shield layer requires seven hours of pouring at 0.68137 m^3/min.

Fig. 16 shows the transient peak saltstone temperatures versus elapsed time from the start pour date for pouring in a vault cell every sixth day. Results are shown for four start pour dates: March 31, June 30, September 30, and December 31. There are a total of twenty-two pour dates. Saltstone is poured eight hours a day for the first twenty pour days. On the twenty-first pour day, saltstone is poured for six hours, and clean cement is poured for seven hours on the twenty-second pour day. 127 days are required to fill the cell. Fig. 16 clearly shows the influence o the seasons on the maximum value of the peak saltstone temperature. With a March 31st start pour date, pouring is completed at the end of July, and the highest peak saltstone temperature exceeds 85º C. With a September 30th start pour date, pouring is completed the first week in February, and the highest peak saltstone temperature is less than 70º C.

Fig. 17 and 18 show the impact of radiolytic heating on the saltstone peak temperature. Results are shown with and without radiolytic heating for the pour scenario described above with a March 31st start pour date. The transient was run for an elapsed time of ten years, and fig. 17 shows the transient peak saltstone temperatures for the two cases. The highest peak temperatures occur 138 days after the commencement of pouring, and pouring is completed on the 127th day. The highest peak temperatures, with and without

radiolytic heating, are 85.80º C and 85.14º C respectively. After ten years, the bulk of the saltstone with radiolytic heating is approximately six degrees Celsius hotter than saltstone without radiolytic heating. After four years, the peak saltstone temperature in the summer is close enough to the saltstone surface to be influenced by the diurnal temperature variation. Fig. 18 shows vertical temperature profiles in the saltstone on July 31st of the ninth year. The temperature in the top 0.2 m of saltstone varies over 24 hours, and during the summer, this is the location of the peak temperature.

The second scenario has pouring in a single vault cell constrained by the 85ºC temperature limit for curing saltstone. Again results are shown for four start pour dates: March 31st, June 30th, September 30th, and December 31st. Pouring is confined to Monday through Friday, and there are again a total of twenty-two pour days. Fig. 19 shows the level of the saltstone surface as a function of elapsed time from the commencement of pouring for the four start pour dates, and the case where pouring occurs five days a week without consideration of the temperature limit. Fig. 20 shows the transient peak saltstone temperatures versus elapsed time from the commencement of pouring for the four start pour dates. Pouring occurs for five consecutive days in the first week, and thereafter there are gaps in the pour schedules to prevent the peak saltstone temperature from exceeding 85º C. Fig. 21 shows vertical temperature profiles in the saltstone at six elapsed times during the pouring and curing process, for the March 31st start pour date.

Pouring five days a week, thirty days are required to fill the cell, and the peak saltstone temperature is 111.6º C. The total volume of saltstone poured is 6786.487 m^3, and the average throughput is 1583.514 m^3/wk. With a March 31st start pour date and a temperature limit of 85º C, ninety-six days are required to fill a cell. The average saltstone throughput is 484.749 m^3/wk. With a June 30th start pour date and a temperature limit of 85º C, one hundred and seven days are required to fill a cell. The average saltstone throughput is 443.976 m^3/wk. With a September 30th start pour date and a temperature limit of 85º C, seventy-nine days are required to fill a cell. The average saltstone throughput is 601.334 m^3/wk. With a December 31st start pour date and a temperature limit of 85º C, sixty days are required to fill a cell. The average saltstone throughput is 791.757 m^3/wk.

Saltstone pouring is rotated between four cells and the cells are filled in two stages in the third scenario. The start pour date is March 31st, and the temperature limit is 85º C. Each stage consists of ten eight hour saltstone pour days, followed by a seven hour pour day for the cement radiation shield layer. No pouring occurs on the weekends. Fig. 22 shows the heights of saltstone in the four cells as functions of elapsed time from the commencement of pouring in the first cell. The elapsed time required to fill four cells is 261 days, and the volume of saltstone poured in the four cells is 26,164.768 m^3. The average pour rate is 701.74 m^3/wk. Fig. 23 shows the transient peak saltstone temperatures in the four cells. Early in a pour stage, the pouring occurs on consecutive days, and the pour schedule late in the stage is adjusted to keep the peak saltstone temperature below the temperature limit of 85 ºC. Fig. 24 shows vertical temperature

profiles in the saltstone in cell #1: at the times of the highest peak temperatures for the two pour stages, just before pouring commences for the second stage, and well after pouring is completed.

Saltstone pouring is rotated between four cells and the cells are filled in three stages in the fourth scenario. The start pour date is March 31st, and the temperature limit is 85º C. The first stage consists of seven saltstone pour days, and the second and third stages consist of six saltstone pour days. Each stage ends with the seven hour pouring of a cement radiation shield layer. Again no pouring occurs on the weekends. Figure 25 shows the heights of saltstone in the four cells as functions of elapsed time from the commencement of pouring in the first cell. The elapsed time required to fill four cells is 191 days, and the volume of saltstone poured in the four cells is 24856.53 m^3. The average pour rate is 910.97 m^3/wk. Fig. 26 shows the transient peak saltstone temperatures in the four cells. Fig. 27 shows vertical temperature profiles in the saltstone in cell #1: at the times of the highest peak temperatures for the three pour stages, just before pouring commences for the second and third stages, and well after pouring is completed.

7. Conclusions

A combination of the heat of hydration of curing saltstone and the allowable temperature limit, restricts the rate at which saltstone can be poured in a single cell. A transient thermal model of the saltstone pouring and curing process has been developed to predict the temperature distributions in saltstone for various pour schedules and seasons of the

year. While there are thermocouple arrays in the vault cells, they cannot be used directly to control the rate of pouring because of the delay between the cessation of pouring and the peak saltstone temperature. Fig. 16 shows the transient peak saltstone temperature for the case in which saltstone is poured into a cell every sixth day. The cell is filled in 127 days, but the peak saltstone temperature occurs 139 days after the commencement of pouring. With a temperature limit, a model is necessary to optimize pour schedules. This is clearly shown in figs. 19 and 20, which show results for pouring in a single cell and an allowable peak saltstone temperature of 85º C. Early in the pour schedule, pouring occurs on consecutive days. The peak saltstone temperature quickly rises to limit, and thereafter remains at or close to the temperature limit until pouring is completed. After approximately the first week, the pour schedule is adjusted to maintain the peak temperature at the limit. 60 days are required to fill the cell with a December 31st start pour date, and 107 days are required to fill the cell with a June 30th start pour date.

The average saltstone pour rate can be increased by filling a cell in multiple stages and rotating the pouring among several cells. With a March 31st start pour date and pouring in a single cell, the average saltstone pour rate is 484.749 m^3/wk. If pouring is rotated among four cells and the cells are filled in two stages with a March 31st start pour date, the average pour rate is 701.74 m^3/wk, and it is 910.97 m3/wk if the cells are filled in three stages. At the end of each pour stage, a 0.3048 m thick layer of cement is poured as a radiation shield. Pouring in multiple stages, results in embedded cement layers that reduce the saltstone capacity of a cell and serve no purpose once the cell is filled.

Nomenclature

A	area, m^2
C_p	specific heat, J/kg K
h	convection heat transfer coefficient, W/m^2 K
h_{rf}	roof convection heat transfer coefficient, W/m^2 K
h_{ss}	saltstone surface convection heat transfer coefficient, W/m^2 K
k	thermal conductivity, W/m K
k_{ss}	saltstone thermal conductivity, W/m K
$\dot{m}_{air}$	ventilation air mass flowrate, kg/s
q^*	internal heat generation rate, W/kg
$\dot{q}_{conv}$	convection heat transfer rate, W/m^2
$\dot{q}_{rad}$	radiation heat transfer rate, W/m^2
t	time, s
T	temperature, K
T_{air}	air temperature, K
T_{airsp}	airspace temperature, K
T_{pl}	pour layer temperature, K
T_{pour}	saltstone pour temperature, K
T_{rf}	lower surface vault roof temperature, K
T_{ss}	saltstone surface temperature, K
V	volume, m^3
Z_{airsp}	height of the airspace, m

Greek letters

Δt	timestep, s
ε_{rf}	roof emissivity
ε_{ss}	saltstone emissivity
Δz	mesh width, m
ρ	density, kg/m^3
σ	Stefan-Boltzmann constant

Acknowledgements

The information contained in this paper was developed during the course of work done under Contract no. DE-AC09-08SR22470 with the US Department of Energy.

References

Anderson, D.A., Tannehill, J.C., Pletcher, R.H. 1984. Computational Fluid Mechanics and Heat Transfer, Hemisphere Publishing Corporation, New York, pp. 56-57.

Duffie, J.A., Beckman, W.A. 1974. Solar Energy Thermal Processes, John Wiley & Sons, New York, p. 76.

Lax, P.D., Richtmyer, R.D., 1956. Survey of the stability of linear finite-difference equations, Communications on Pure and Applied Mathematics 9, 267-293.

Figures:

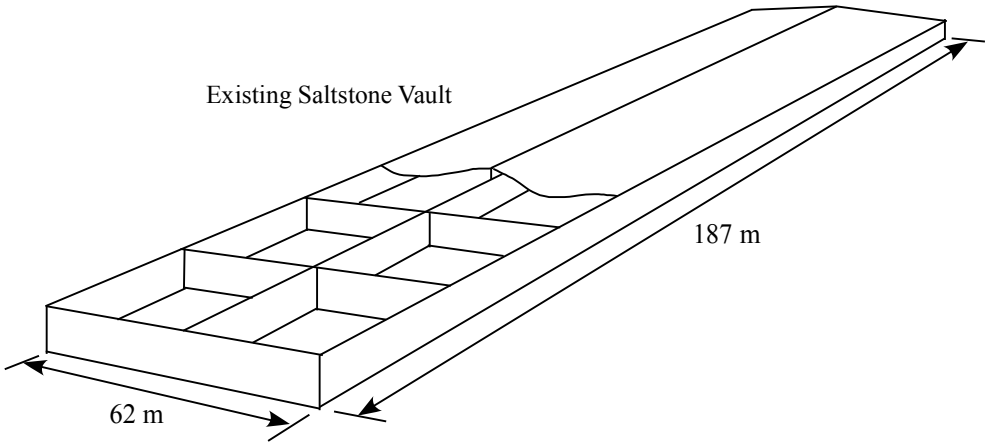

Fig. 1

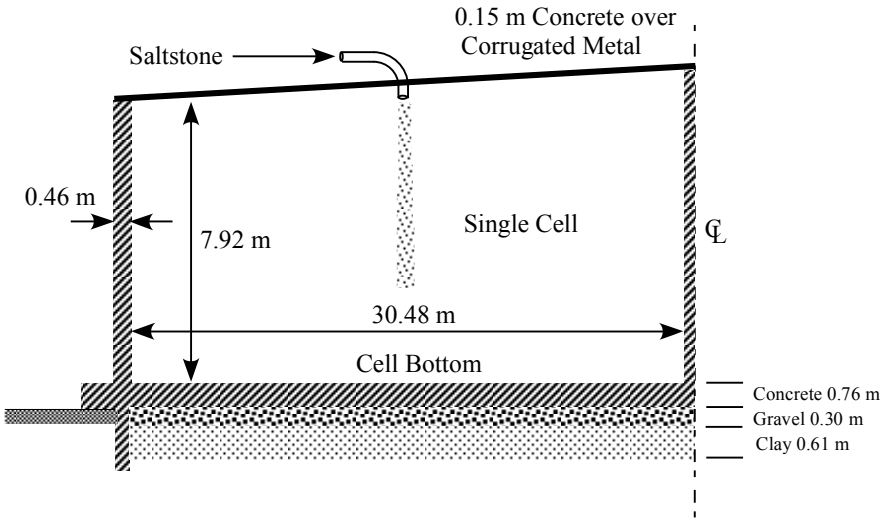

Fig. 2

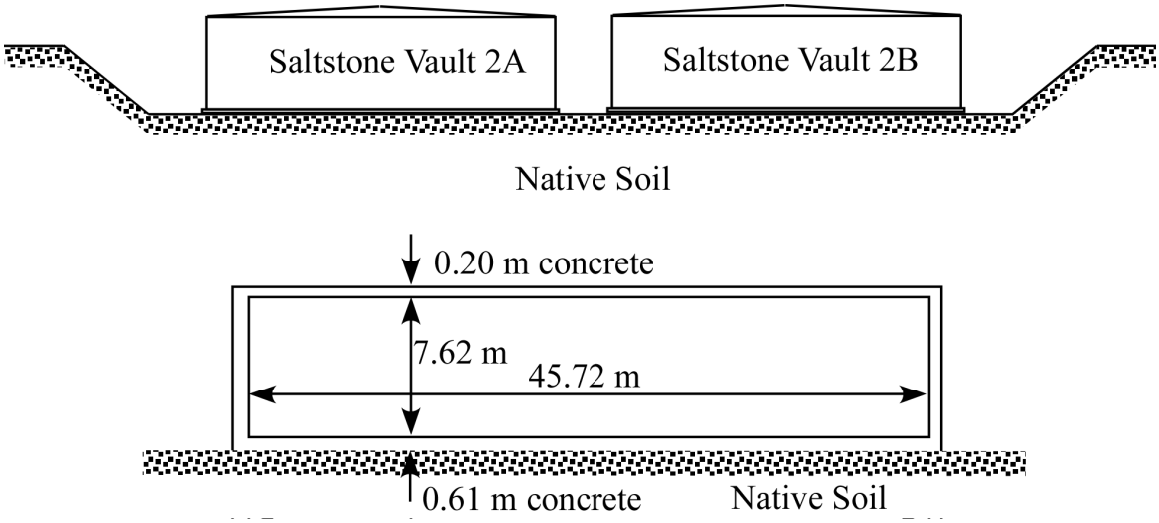
Saltstone Vault 2A
Saltstone Vault 2B
Native Soil
0.20 m concrete
7.62 m
45.72 m
0.61 m concrete
Native Soil

Fig. 3

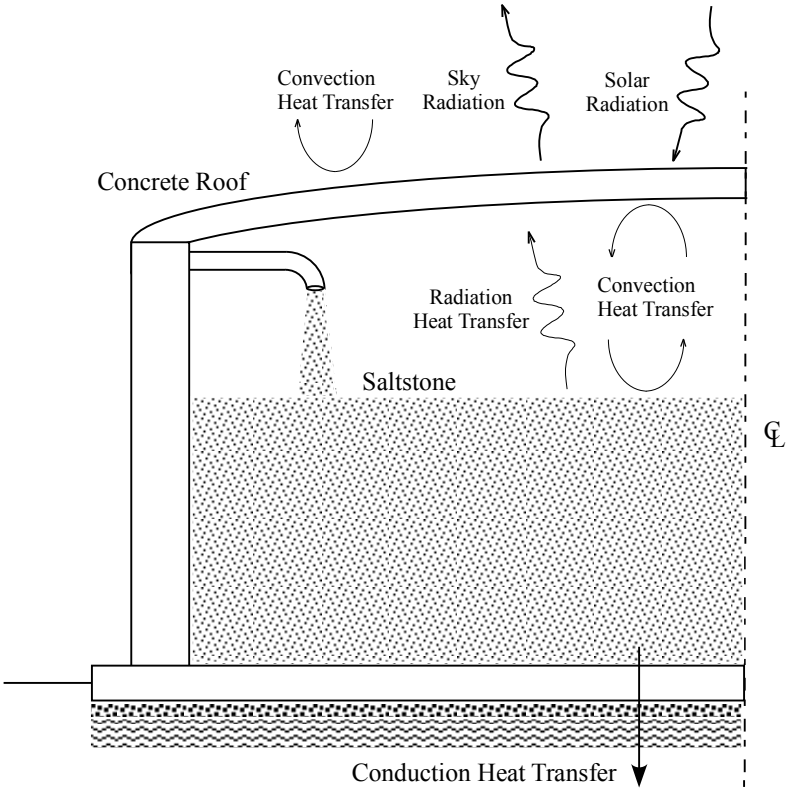
Convection
Heat Transfer
Sky
Radiation
Solar
Radiation
Concrete Roof
Radiation
Heat Transfer
Convection
Heat Transfer
Saltstone
℄
Conduction Heat Transfer

Fig. 4

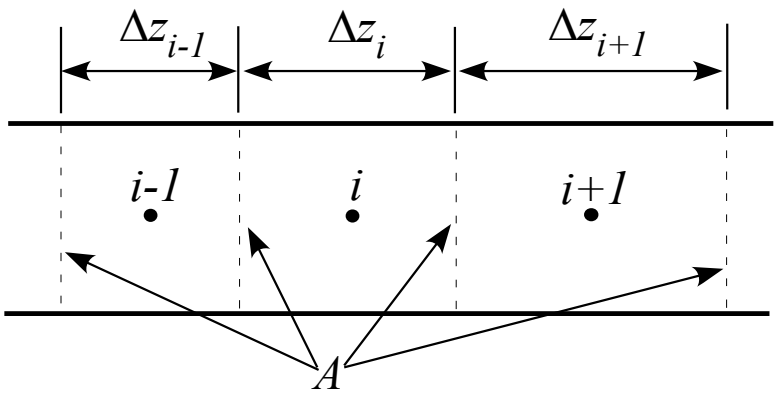
Δz_{i-1}
Δz_i
Δz_{i+1}
i-1
i
i+1
A

Fig. 5

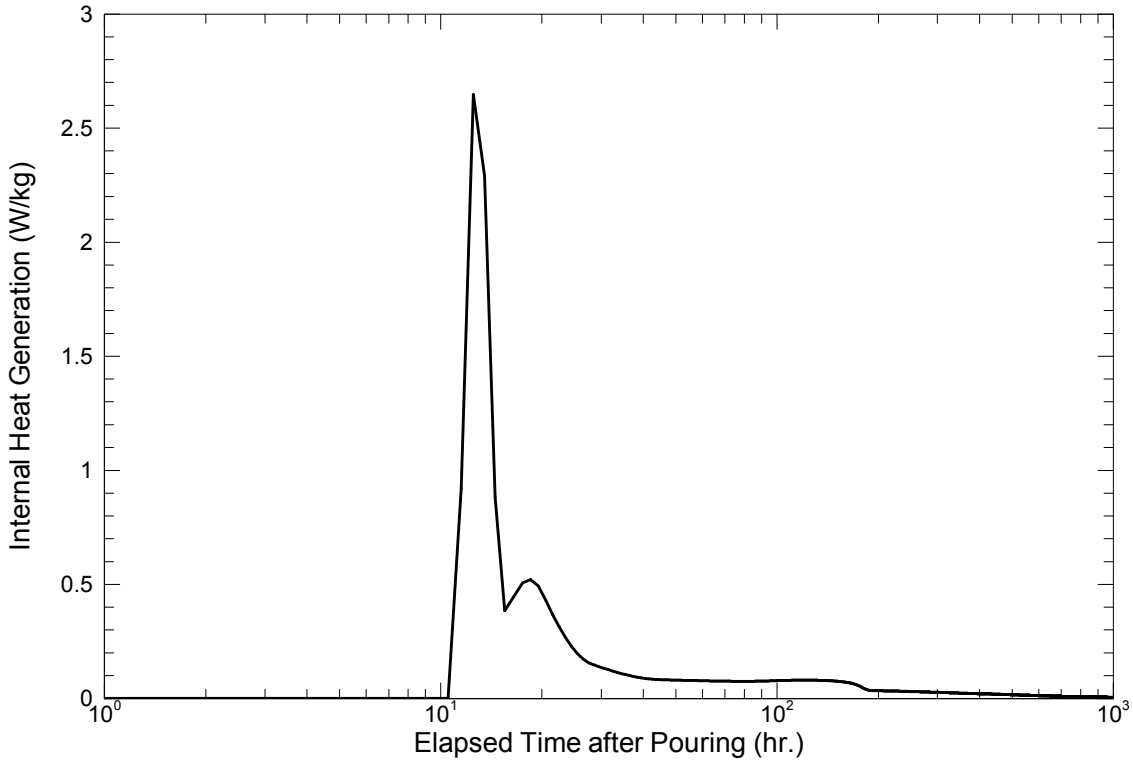
Internal Heat Generation (W/kg)
Elapsed Time after Pouring (hr.)
0
0.5
1
1.5
2
2.5
3
10^0
10^1
10^2
10^3

Fig. 6

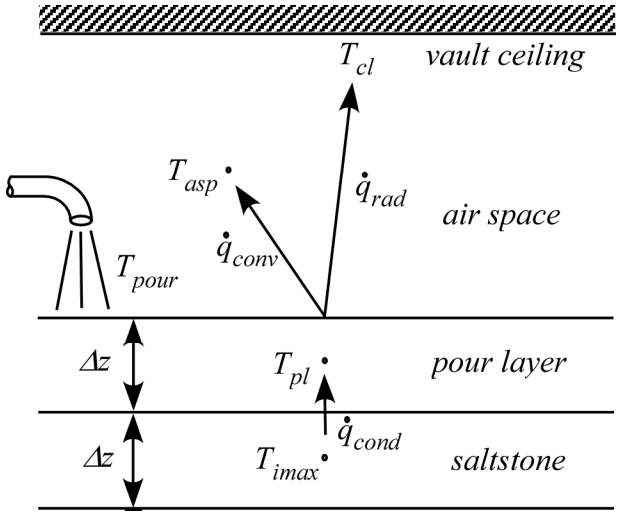
T_{cl}
vault ceiling
T_{asp}
$\dot{q}_{rad}$
air space
$\dot{q}_{conv}$
T_{pour}
Δz
T_{pl}
pour layer
$\dot{q}_{cond}$
Δz
T_{imax}
saltstone

Fig. 7

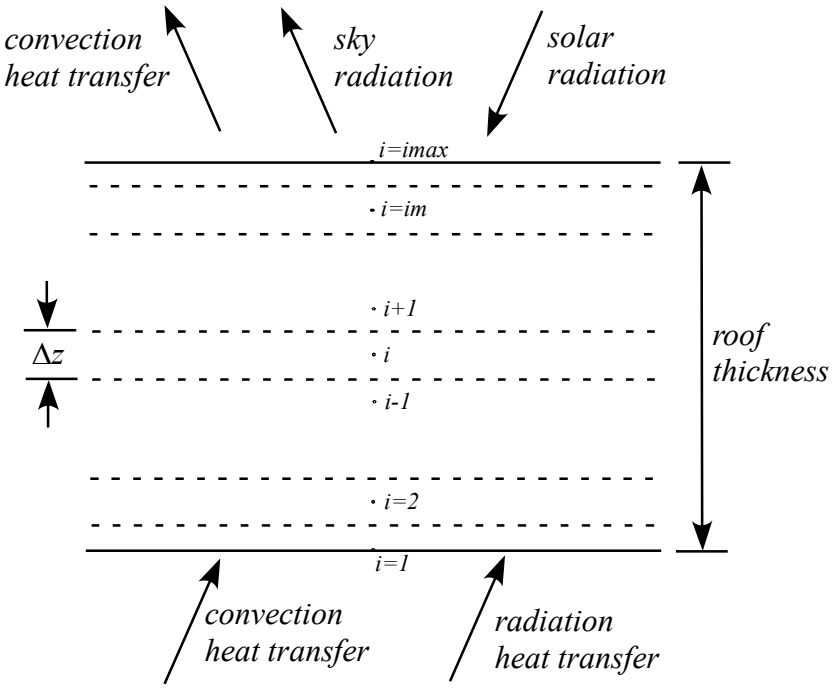
convection
heat transfer
sky
radiation
solar
radiation
i=imax
i=im
i+1
Δz
i
i-1
roof
thickness
i=2
i=1
convection
heat transfer
radiation
heat transfer

Fig. 8

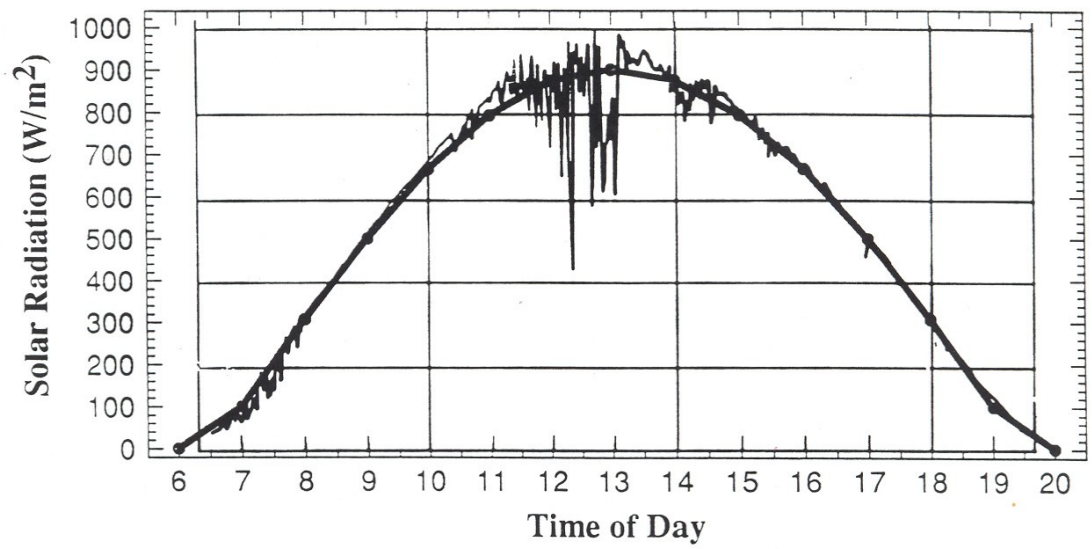
Solar Radiation (W/m2)
1000
900
800
700
600
500
400
300
200
100
0
6
7
8
9
10
11
12
13
14
15
16
17
18
19
20
Time of Day

Fig. 9

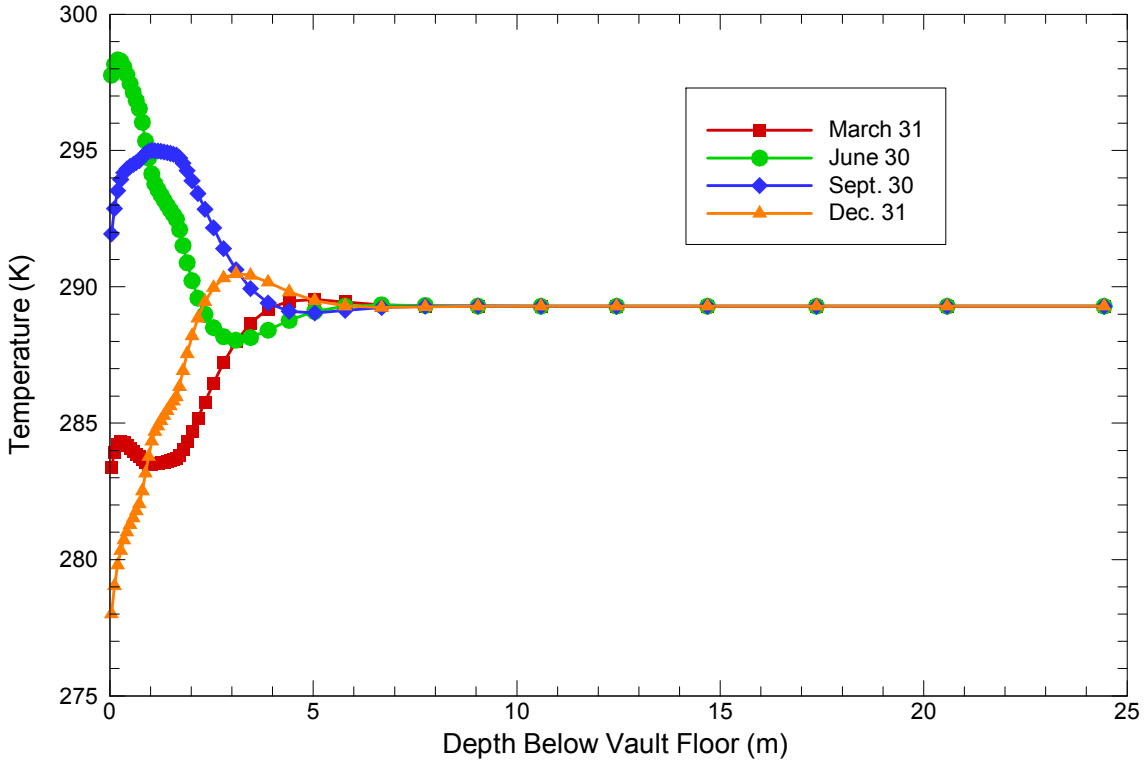
Temperature (K)
300
295
290
285
280
275
0
5
10
15
20
25
Depth Below Vault Floor (m)
March 31
June 30
Sept. 30
Dec. 31

Fig. 10

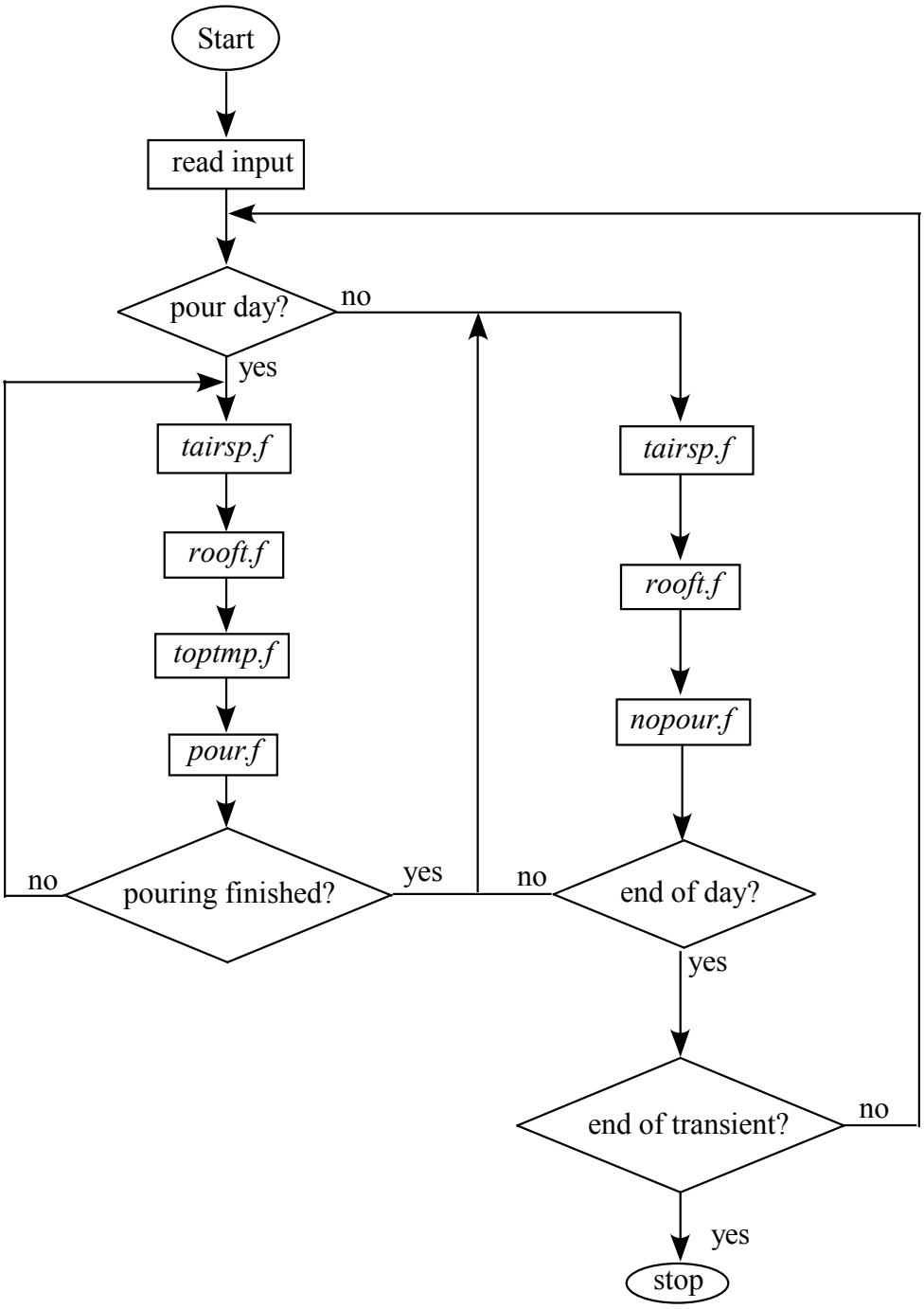
Start
read input
pour day?
no
yes
tairsp.f
rooft.f
toptmp.f
pour.f
pouring finished?
no
yes
tairsp.f
rooft.f
nopour.f
no
end of day?
yes
end of transient?
no
yes
stop

Fig. 11

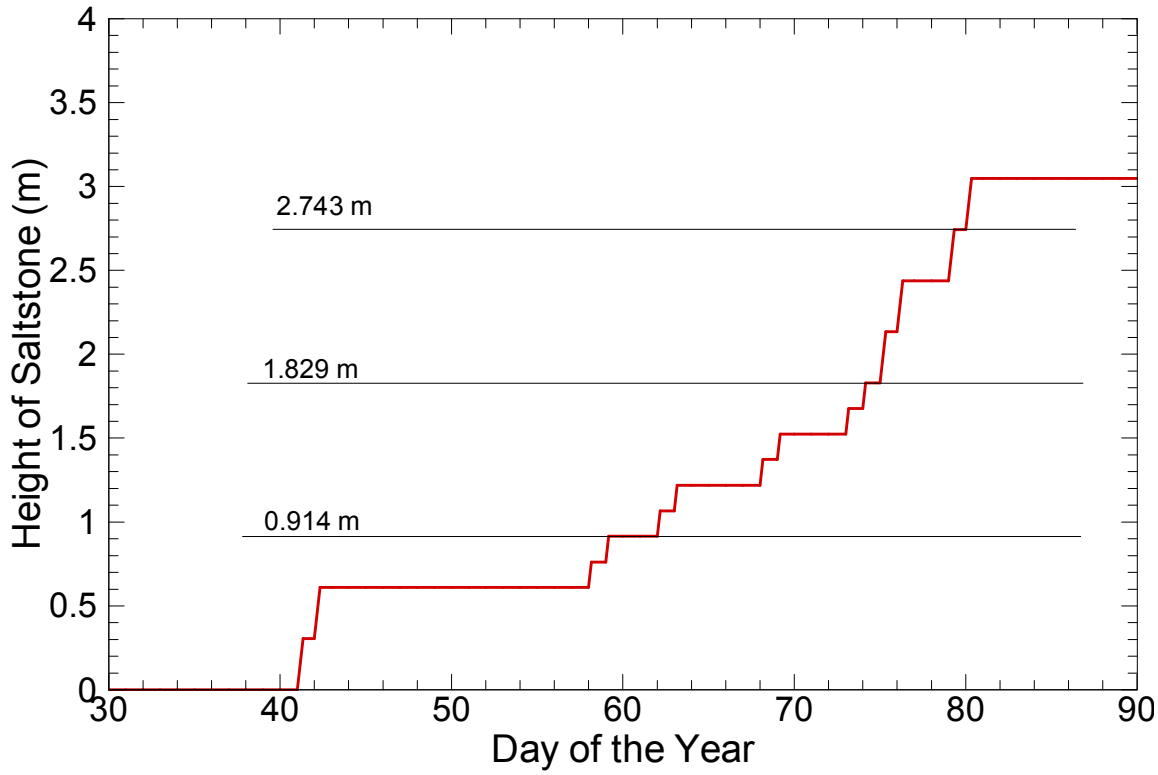
Height of Saltstone (m)
Day of the Year
2.743 m
1.829 m
0.914 m
0
0.5
1
1.5
2
2.5
3
3.5
4
30
40
50
60
70
80
90

Fig. 12

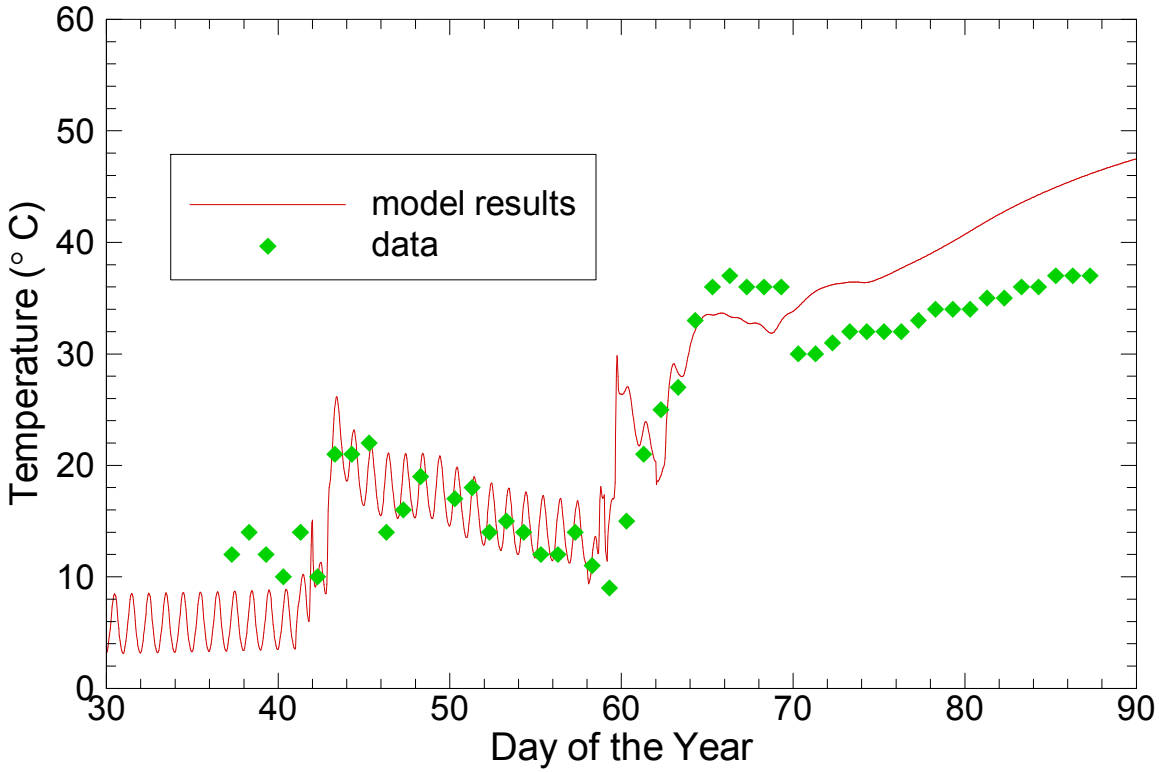
Temperature (° C)
Day of the Year
model results
data
0
10
20
30
40
50
60
30
40
50
60
70
80
90

Fig. 13

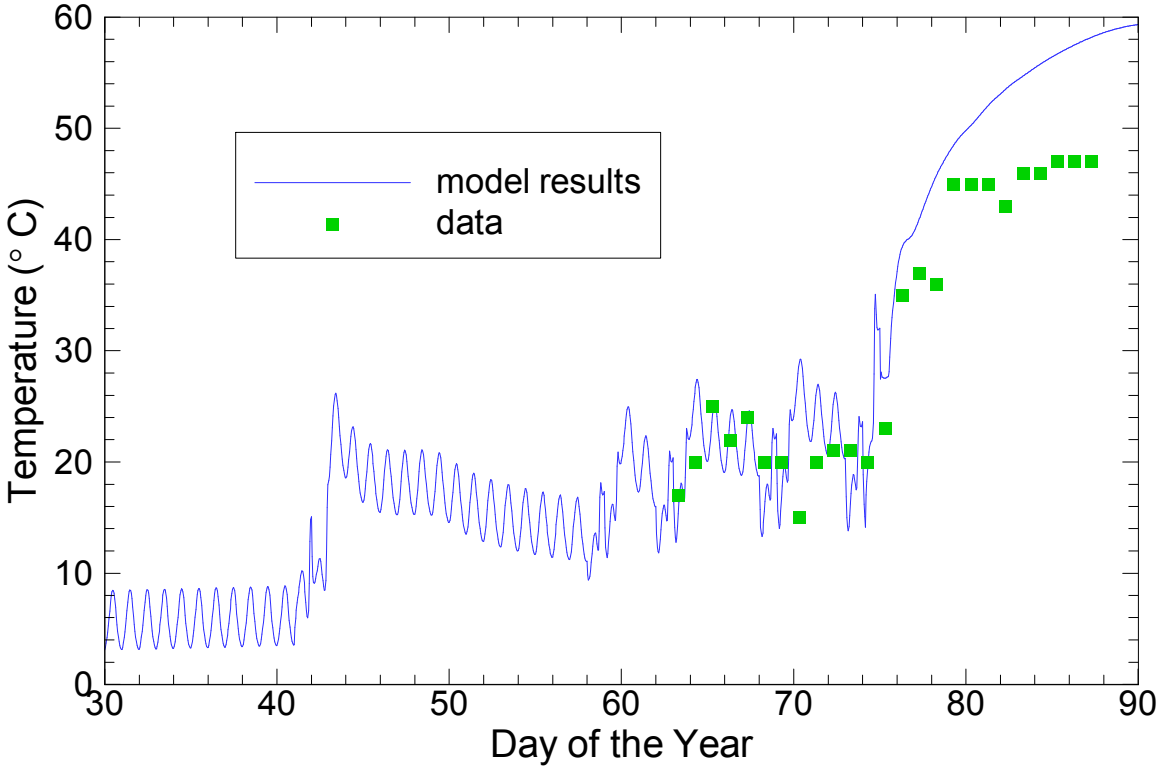
model results
data
Temperature (° C)
Day of the Year
0
10
20
30
40
50
60
30
40
50
60
70
80
90

Fig. 14

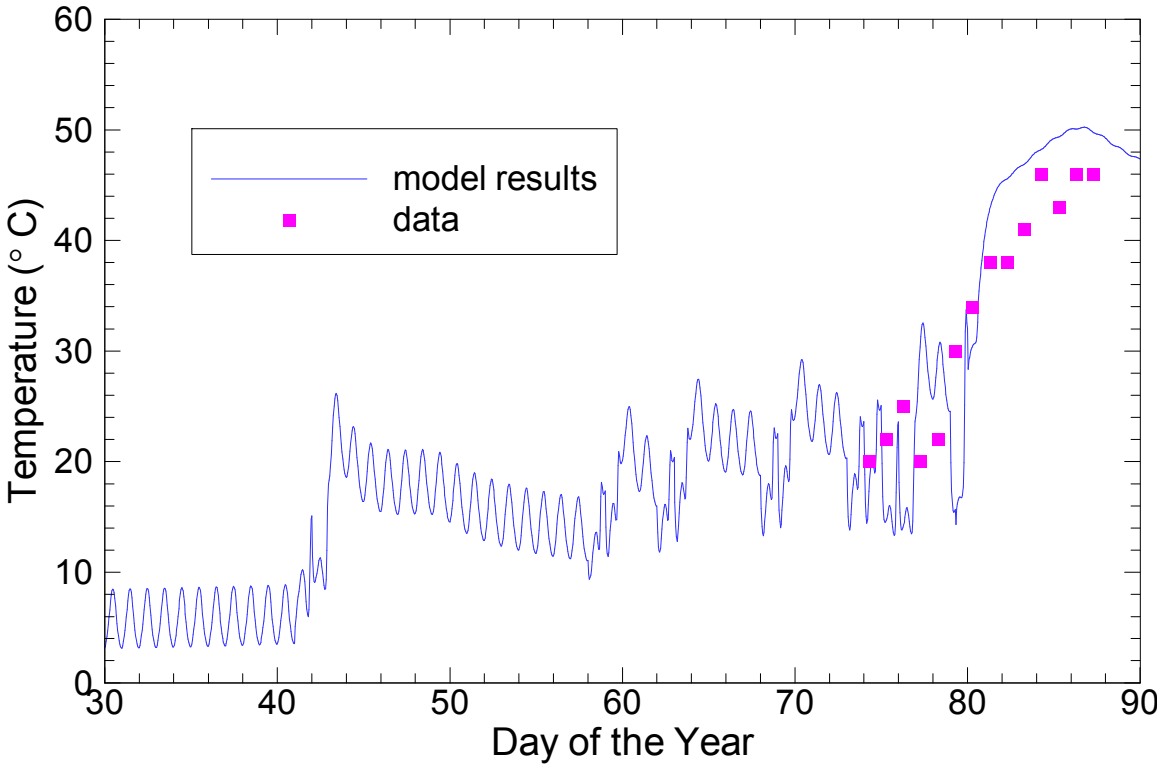
model results
data
Temperature (° C)
Day of the Year
0
10
20
30
40
50
60
30
40
50
60
70
80
90

Fig. 15

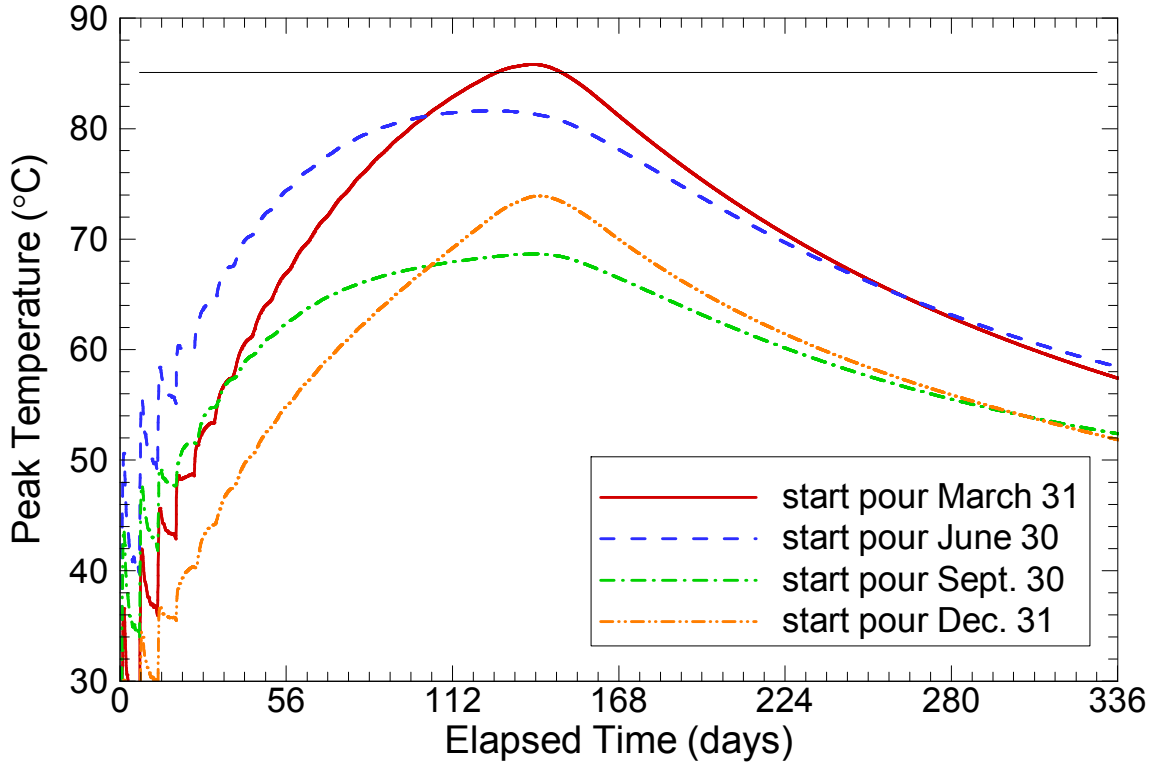
Peak Temperature (°C)
Elapsed Time (days)
start pour March 31
start pour June 30
start pour Sept. 30
start pour Dec. 31
90
80
70
60
50
40
30
0
56
112
168
224
280
336

Fig. 16

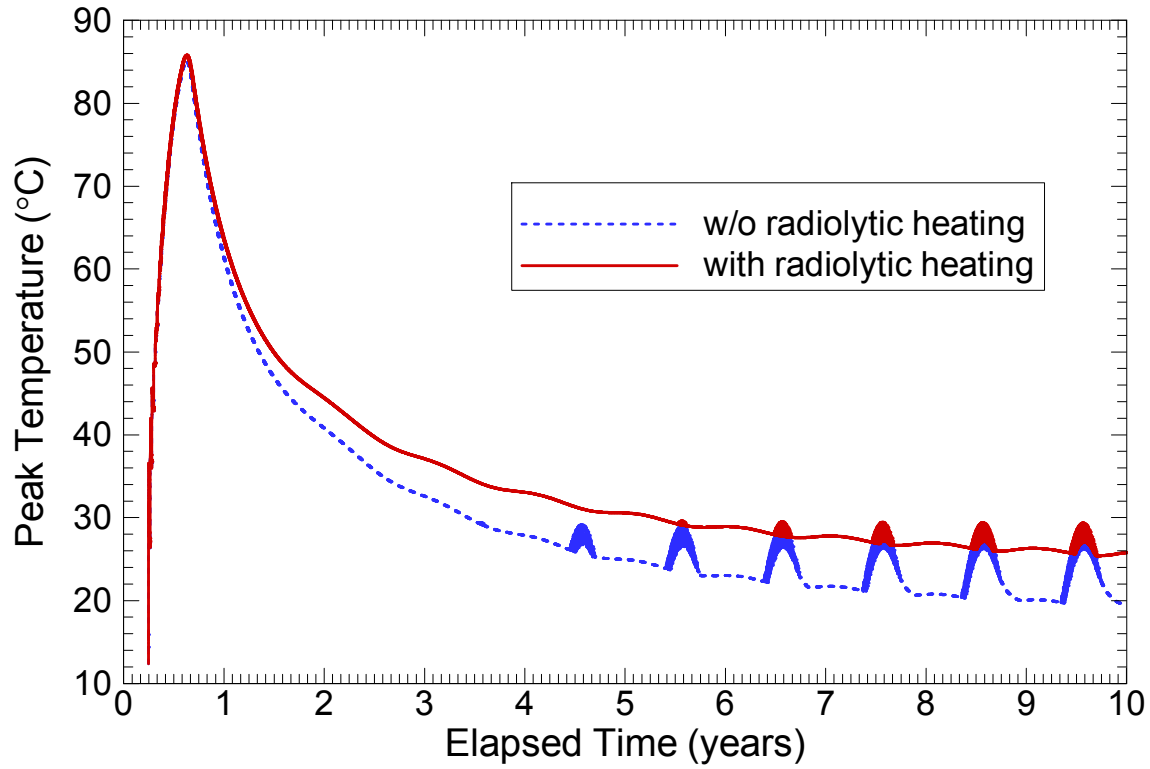
Peak Temperature (°C)
Elapsed Time (years)
w/o radiolytic heating
with radiolytic heating
90
80
70
60
50
40
30
20
10
0
1
2
3
4
5
6
7
8
9
10

Fig. 17

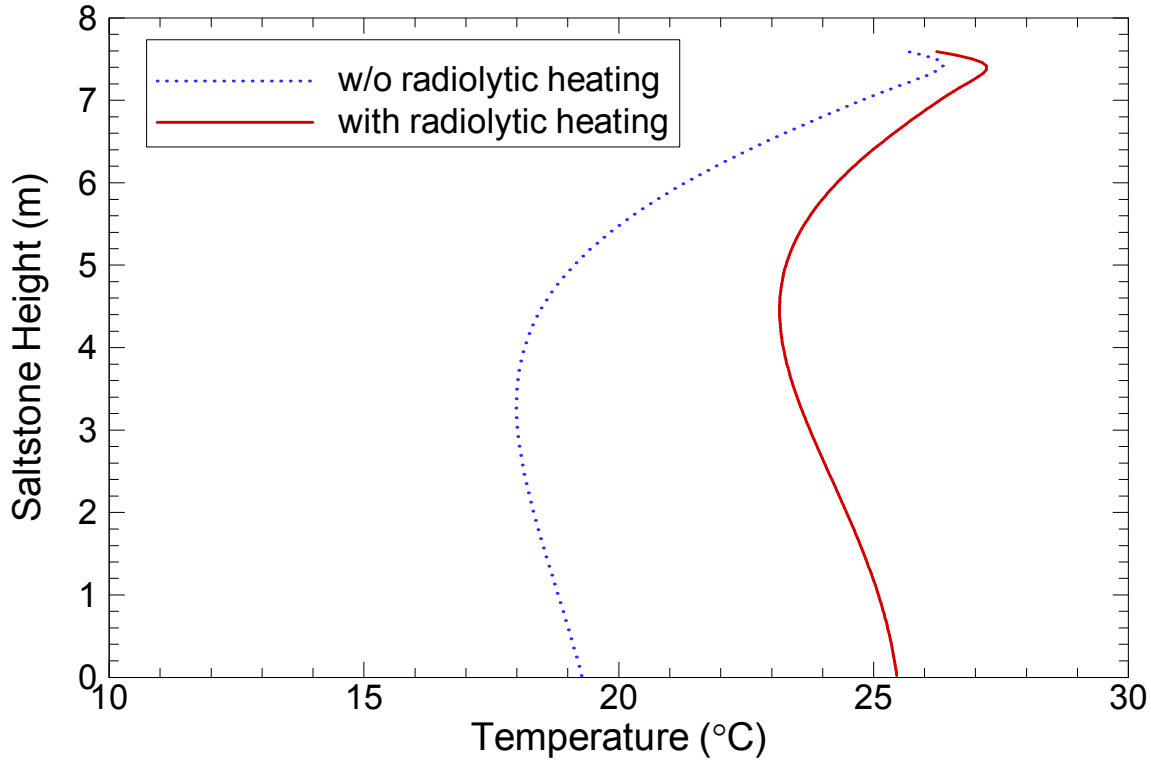
w/o radiolytic heating
with radiolytic heating
Saltstone Height (m)
Temperature (°C)
0
1
2
3
4
5
6
7
8
10
15
20
25
30

Fig. 18

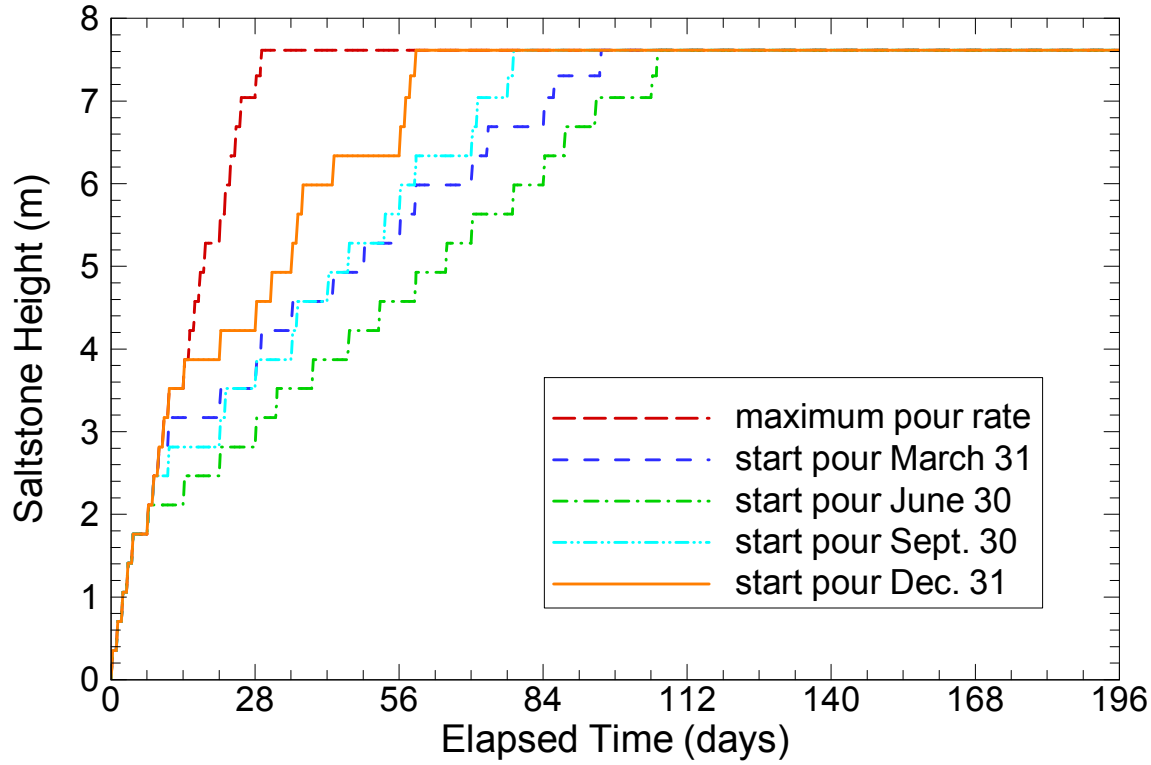
maximum pour rate
start pour March 31
start pour June 30
start pour Sept. 30
start pour Dec. 31
Saltstone Height (m)
Elapsed Time (days)
0
1
2
3
4
5
6
7
8
0
28
56
84
112
140
168
196

Fig. 19

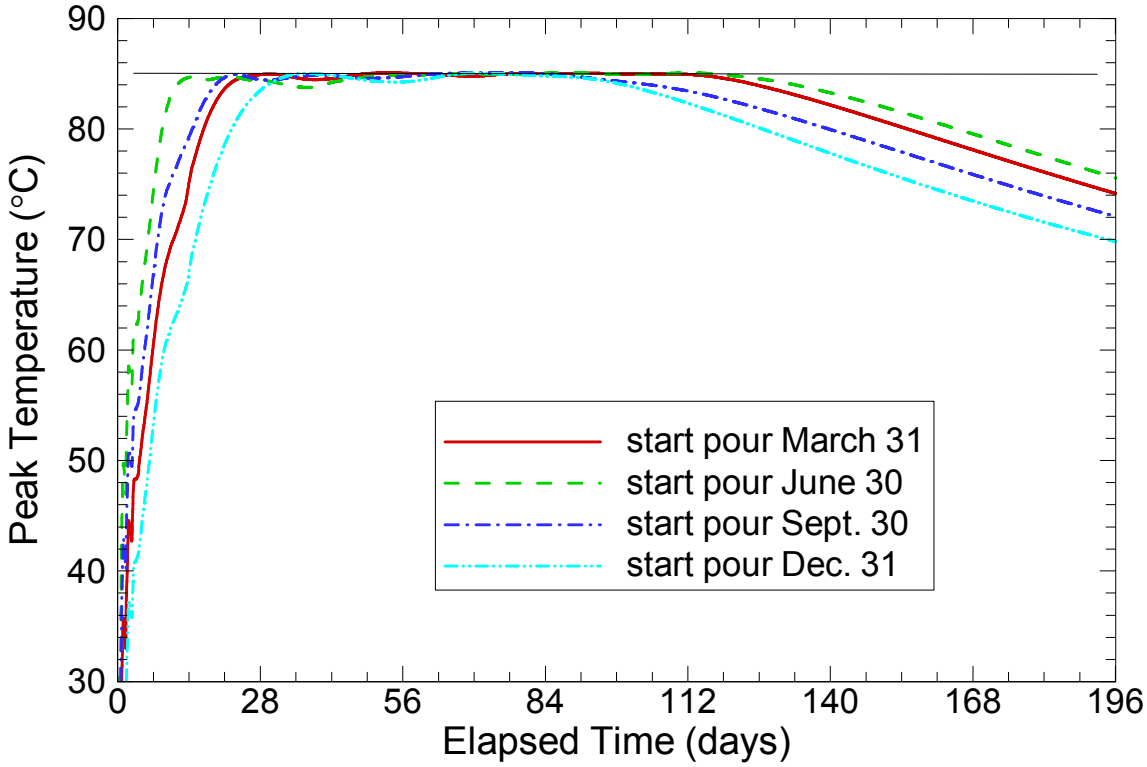
Peak Temperature (°C)
Elapsed Time (days)
start pour March 31
start pour June 30
start pour Sept. 30
start pour Dec. 31
90
80
70
60
50
40
30
0
28
56
84
112
140
168
196

Fig. 20

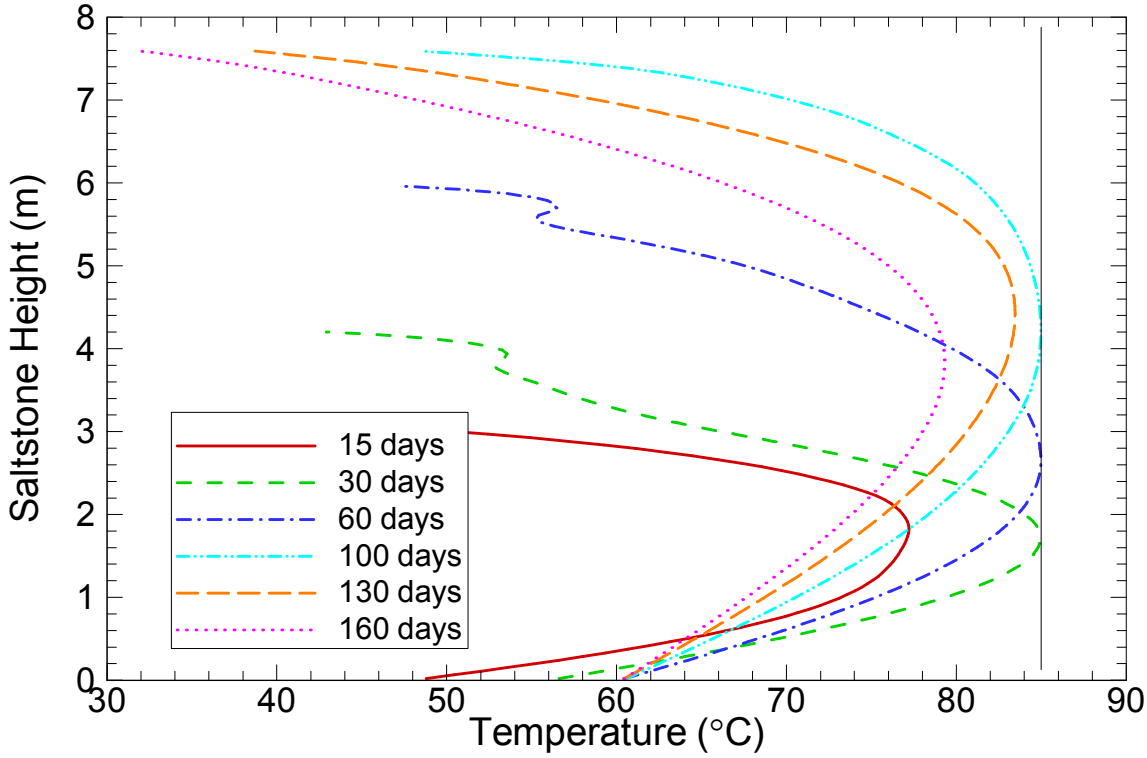
Saltstone Height (m)
Temperature (°C)
15 days
30 days
60 days
100 days
130 days
160 days
8
7
6
5
4
3
2
1
0
30
40
50
60
70
80
90

Fig. 21

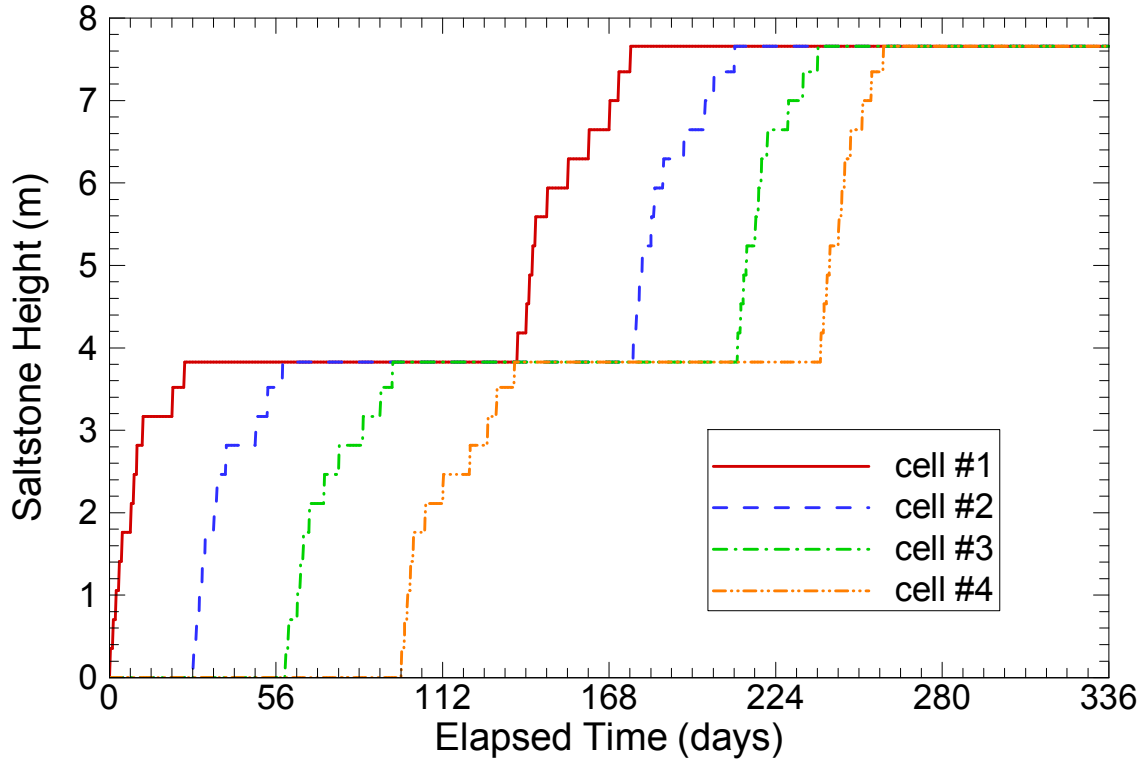
Saltstone Height (m)
Elapsed Time (days)
0
1
2
3
4
5
6
7
8
0
56
112
168
224
280
336
cell #1
cell #2
cell #3
cell #4

Fig. 22

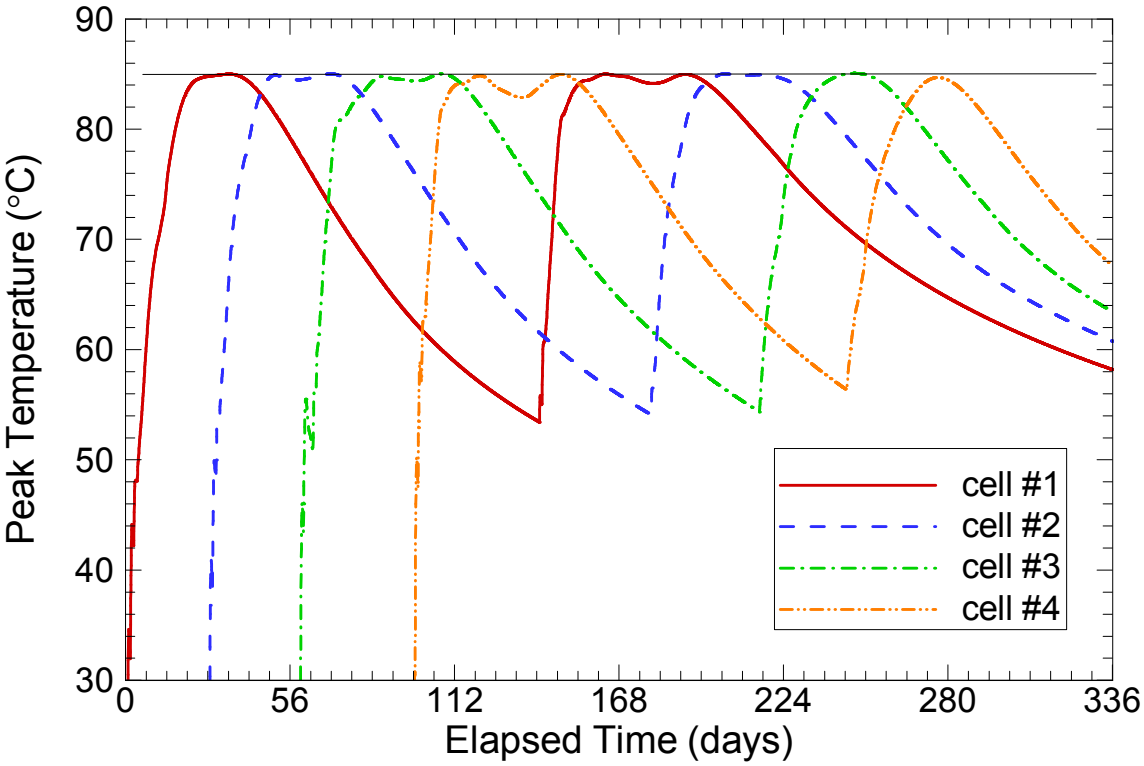
Peak Temperature (°C)
Elapsed Time (days)
30
40
50
60
70
80
90
0
56
112
168
224
280
336
cell #1
cell #2
cell #3
cell #4

Fig. 23

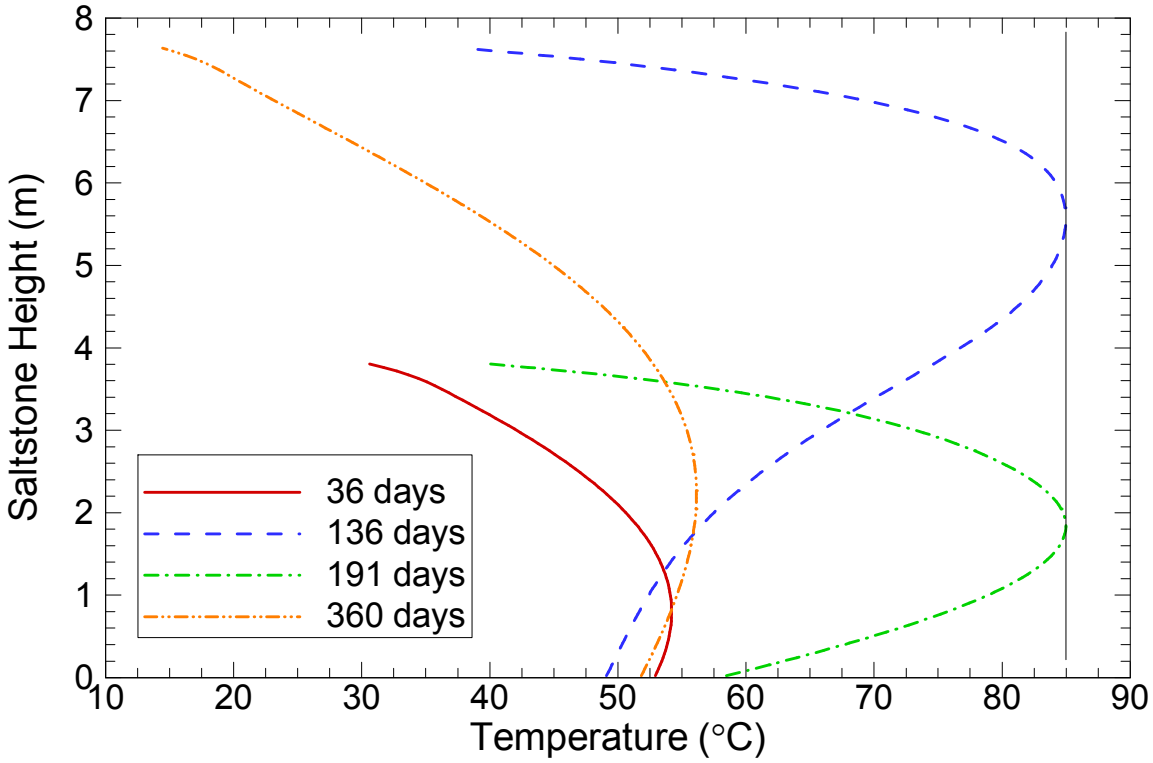
Saltstone Height (m)
Temperature (°C)
36 days
136 days
191 days
360 days

Fig. 24

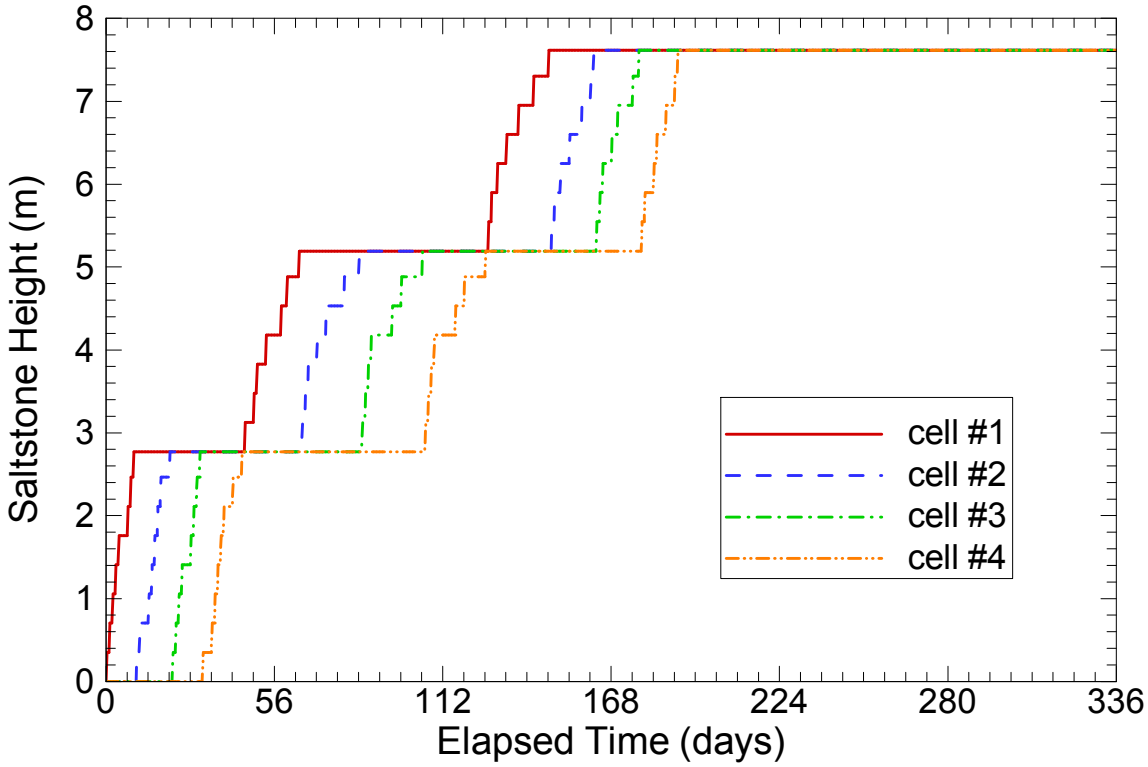
Saltstone Height (m)
Elapsed Time (days)
cell #1
cell #2
cell #3
cell #4

Fig. 25

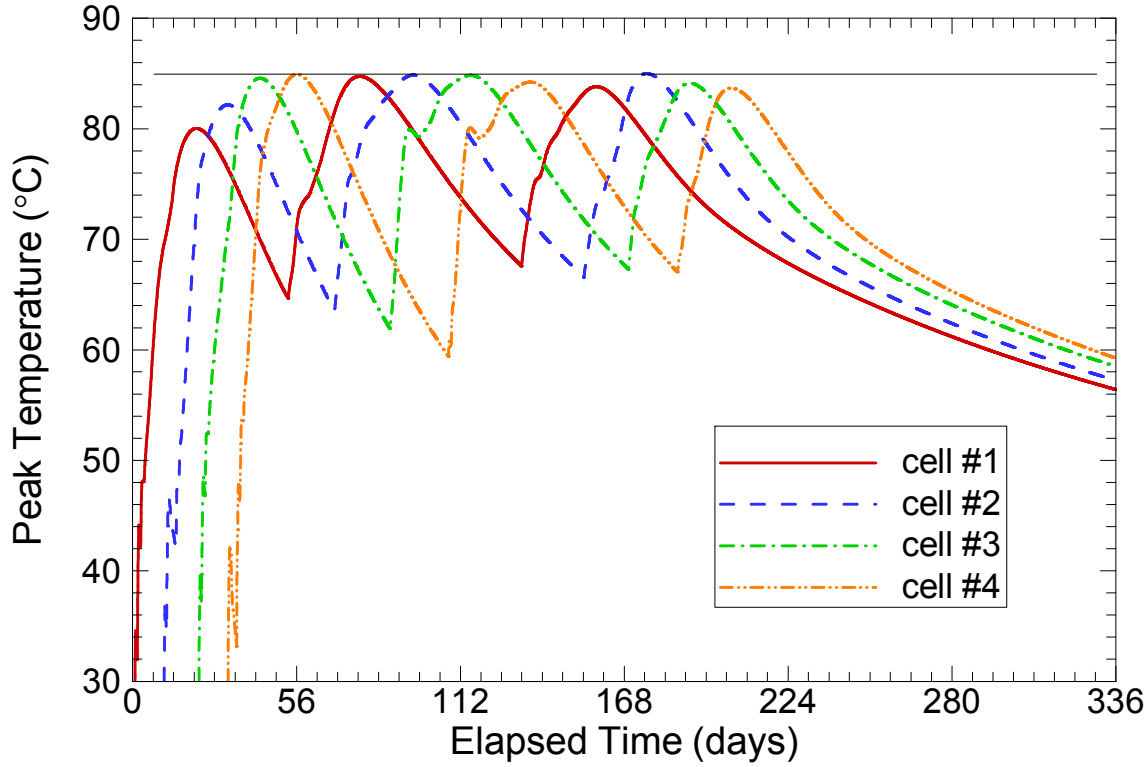
Peak Temperature (°C)
Elapsed Time (days)
cell #1
cell #2
cell #3
cell #4
90
80
70
60
50
40
30
0
56
112
168
224
280
336

Fig. 26

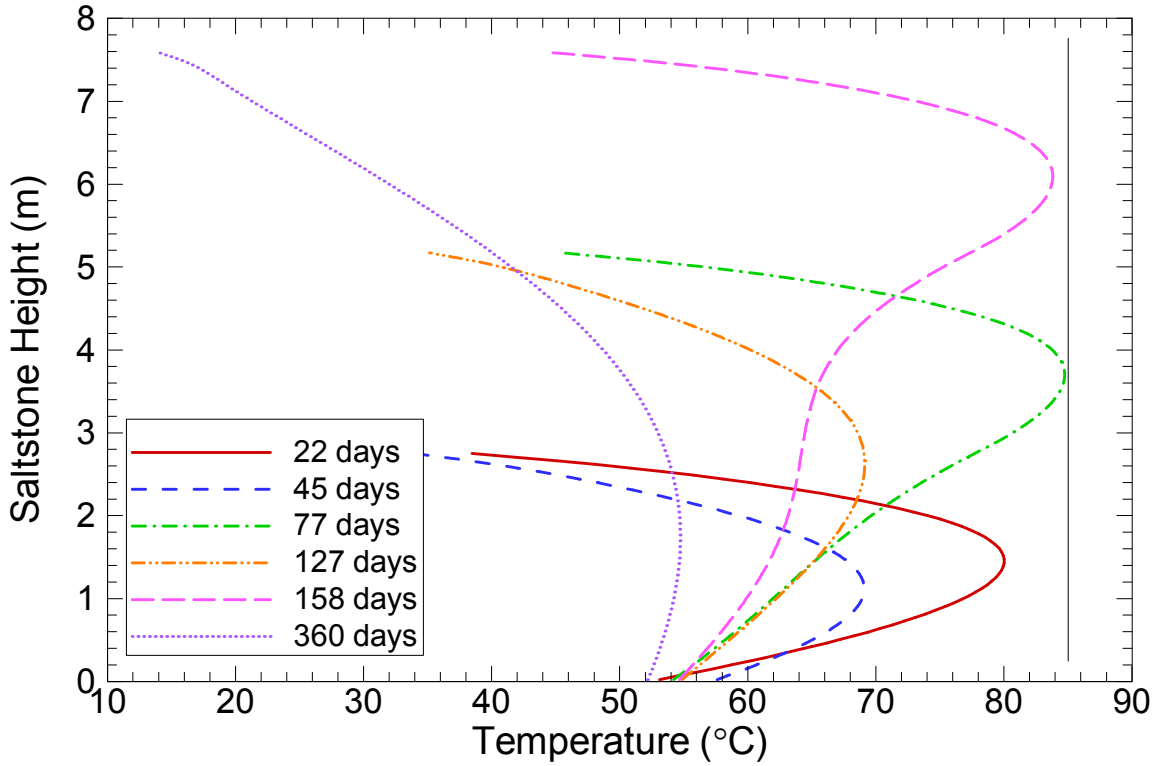
Saltstone Height (m)
Temperature (°C)
22 days
45 days
77 days
127 days
158 days
360 days
8
7
6
5
4
3
2
1
0
10
20
30
40
50
60
70
80
90

Fig. 27

Captions:

Fig. 1: Schematic of the existing saltstone vault.

Fig. 2: Vertical cross-section of a single cell in the existing vault.

Fig. 3: Schematic of the vault #2 design.

Fig. 4: Vault schematic showing the heat transfer mechanisms cooling the saltstone.

Fig. 5: A one-dimensional variable width mesh.

Fig. 6: Saltstone internal heat generation rate, due to the heat of hydration of the curing saltstone, as a function of elapsed time after mixing.

Fig. 7: Schematic of the pour layer heat transfer.

Fig. 8: Schematic of the vault concrete roof showing the nodalization and boundary conditions.

Fig. 9: Total solar radiation on a horizontal surface vs time on a clear day Greenbelt, Maryland on May 14, 1971, [5].

Fig. 10: Initial temperature distributions in the ground below a vault as a function of the start pour date.

Fig. 11: Flowchart of the saltstone thermal pour model *sspour.f*.

Fig. 12: Height of saltstone surface versus elapsed time between January 31st and March 30th.

Fig. 13: Predicted and measured saltstone temperatures by the thermocouple at the elevation 0.914 m.

Fig. 14: Predicted and measured saltstone temperatures by the thermocouple at the elevation 1.829 m.

Fig. 15: Predicted and measured saltstone temperatures by the thermocouple at the elevation 2.743 m.

Fig. 16: Saltstone peak temperatures vs elapsed time from the commencement of pouring, for four start pour dates. Every sixth day saltstone is poured for eight hours.

Fig. 17: Transient saltstone peak temperatures with and without radiolytic heating. Pouring occurs every sixth day for eight hours, and the start pour date is

March 31st.

Fig. 18: Saltstone vertical temperature profiles with and without radiolytic heating on March 31st of the ninth year after pouring.

Fig. 19: Saltstone depth vs elapsed time from the commencement of pouring for four start pour dates. Pouring occurs in a single cell and the saltstone temperature limit is 85.0 ºC.

Fig. 20: Saltstone peak temperatures vs elapsed time from the commencement of pouring, for four start pour dates and the saltstone temperature limit is 85.0 ºC.

Fig. 21: Saltstone vertical temperature profiles at six elapsed times from the commencement of pouring. Saltstone is poured in a single cell and the start pour date is March 31.

Fig. 22: Saltstone depth vs elapsed time from the commencement of pouring. Pouring is rotated between four cells and in two stages per cell. The start pour date is March 31 and the saltstone temperature limit is 85.0 ºC.

Fig. 23: Saltstone peak temperatures vs elapsed time from the commencement of Pouring. Pouring is rotated between four cells and in two stages per cell. The start pour date is March 31 and the saltstone temperature limit is 85.0 ºC.

Fig. 24: Saltstone vertical temperature profiles in cell #1 at four elapsed times from the commencement of pouring. The start pour date is March 31 and the saltstone temperature limit is 85.0 ºC.

Fig. 25: Saltstone peak temperatures vs elapsed time from the commencement of Pouring. Pouring is rotated between four cells and in three stages per cell. The start pour date is March 31 and the saltstone temperature limit is 85.0 ºC.

Fig. 26: Saltstone peak temperatures vs elapsed time from the commencement of Pouring. Pouring is rotated between four cells and in three stages per cell. The start pour date is March 31 and the saltstone temperature limit is 85.0 ºC.

Fig. 27: Saltstone vertical temperature profiles in cell #1 at six elapsed times from the commencement of pouring. The start pour date is March 31 and the saltstone temperature limit is 85.0 ºC.